Streaming potential dependence on water-content in Fontainebleau sand

Vincent Allègre, Laurence Jouniaux, François Lehmann, Pascal Sailhac

Geophysical Journal International

Geophys. J. Int. (2010) **182,** 1248–1266 doi: 10.1111/j.1365-246X.2010.04716.x

Streaming potential dependence on water-content in Fontainebleau sand

V. Allègre,[1] L. Jouniaux,[1] F. Lehmann[2] and P. Sailhac[1]

[1]*Institut de Physique du Globe de Strasbourg, UdS-CNRS UMR* 7516 *Université de Strasbourg,* 5 *rue rené Descartes,* 67084 *Strasbourg, France. E-mail: vincent.allegre@unistra.fr*

[2]*Laboratoire d'Hydrologie et de Géochimie de Strasbourg, UdS-CNRS UMR* 7517 *Université de Strasbourg,* 1 *rue Blessig,* 67000 *Strasbourg, France*

Accepted 2010 June 26. Received 2010 June 25; in original form 2009 October 7

SUMMARY

The electrokinetic potential results from the coupling between the water flow and the electrical current because of the presence of ions within water. The electrokinetic coefficient is well described in fluid-saturated media, however its behaviour under unsaturated flow conditions is still discussed. We propose here an experimental approach to investigate streaming potential variations in sand at unsaturated conditions. We present for the first time continuous records of the electrokinetic coefficient as a function of water content. Two drainage experiments have been performed within a column filled with a clean sand. Streaming potential measurements are combined with water pressure and water content measurements every 10 cm along the column. In order to model hydrodymanics during the experiments, we solve Richards equation coupled with an inverse problem to estimate the hydraulic parameters of the constitutive relations between hydraulic conductivity, water pressure and water content. The electrokinetic coefficient C shows a more complex behaviour for unsaturated conditions than it was previously reported and cannot be fitted by the existing models. The normalized electrokinetic coefficient increases first when water saturation decreases from 100 to about 65–80 per cent, and then decreases as the water saturation decreases, whereas all previous works described a monotone decrease of the normalized electrokinetic coupling as water saturation decreases. We delimited two water saturation domains, and deduced two different empirical laws describing the evolution of the electrokinetic coefficient for unsaturated conditions. Moreover, we introduce the concept of the electrokinetic residual saturation, $S_{\mathrm{w}}^{\mathrm{r,ek}}$, which allows us to propose a new model derived from the approach of the relative permeability used in hydrodynamics.

Key words: Electrical properties; Hydrogeophysics; Hydrology; Permeability and porosity; Fracture and flow.

1 INTRODUCTION

The self-potential (SP) method is a passive geophysical method based on the natural occurrence of electric fields on the Earth's surface. The SP anomalies are usually explained by the electrokinetic, electrochemical and thermoelectric effects (Marshall & Madden 1959). Therefore, the SP method has been used for a variety of geophysical applications. The SP method has been used to image contaminant plumes (Naudet *et al.* 2003), and to detect salt concentration fronts (Maineult *et al.* 2004, 2005). Numerous SP observations are interpreted through the electrokinetic coupling, for instance to characterize geothermal and volcanic areas (Finizola *et al.* 2002, 2004). However, the electrokinetic origin involved to explain the positive SP anomalies observed on active volcanoes is still under debate (Ishido 2004; Onizawa *et al.* 2009).

Recent models on electrokinetics have been proposed for reservoir geophysics and petroleum investigations (Jackson 2008; Saunders *et al.* 2008), and self-potentials have been monitored during hydraulic tests in boreholes (Marquis *et al.* 2002; Darnet *et al.* 2006; Maineult *et al.* 2008). Moreover recent developments allow us to use SP measurements in boreholes as an electrical flowmeter (Pezard *et al.* 2009). The electrokinetic coupling is also directly involved in seismo-electromagnetic effects (Pride 1994; Garambois & Dietrich 2001, 2002; Bordes *et al.* 2006; Strahser *et al.* 2007; Bordes *et al.* 2008).

For hydrological applications, Bogolovsky & Ogilvy (1970) described a method to infer water table variations from self-potential measurements. Moreover, the inversion of SP observations can yield an estimate of the vadose zone hydraulic properties (Gibert & Pessel 2001; Sailhac & Marquis 2001; Darnet *et al.* 2003; Sailhac *et al.* 2004; Titov *et al.* 2005). However, inferring a firm link between SP intensity and water flux (Jouniaux *et al.* 1999; Doussan *et al.* 2002; Darnet & Marquis 2004) or deformation (Jouniaux *et al.* 1994; Henry *et al.* 2003) is difficult, although it has been proposed to predict permeability using electrokinetic theory (Glover *et al.* 2006; Glover & Walker 2009).

Electrokinetic contribution to self-potentials takes its origin in the electrical double-layer (EDL), or electrical triple-layer (Davis *et al.* 1978), which is located at the electrolyte/grain interface of a saturated porous media. This concept has been first introduced by Stern (1924), and then modelled and improved by electrochemists (Overbeek 1952; Dukhin & Derjaguin 1974). The electrokinetic coefficient is defined as the ratio between the macroscopic induced electrical potential and the driving pore pressure. Indeed the water flow carries the ions present in the water and can induce an electrical current. The electrokinetic coefficient depends on some fluid parameters, as electrical conductivity and dynamic viscosity, and on the so-called zeta potential (ζ) (Smoluchowski 1905), which is the electrical potential at the shear plane of the EDL. Its understanding is crucial for electrokinetics. The ζ potentials inferred from streaming potential measurements on crushed samples have been reported as a function of pH (Ishido & Mizutani 1981; Hase *et al.* 2003), temperature (Ishido & Mizutani 1981; Tosha *et al.* 2003), and mineral composition (Massenet & Pham 1985; Morgan *et al.* 1989; Pozzi & Jouniaux 1994; Guichet *et al.* 2006). The influence of the fluid electrical conductivity has also been investigated (Pride & Morgan 1991; Lorne *et al.* 1999a; Jouniaux *et al.* 2000). It is usually reported that variations of electrical conductivity from 0.001 to 1 S m^{-1} induces a three orders of magnitude change of the electrokinetic coefficient.

However, the variation of the electrokinetic coefficient with saturation is still discussed and not yet understood. The interpretation of SP observations applied to reservoir geophysics requires a good estimation of the electrokinetic coefficient in unsaturated conditions (Jackson 2008; Maineult *et al.* 2008). Moreover the influence of water content on seismoelectromagnetics is still not known. Experimental measurements on streaming potentials as a function of water content within sand showed that the electrokinetic coefficient decreases when water saturation decreases (Guichet *et al.* 2003) and showed that this coefficient is roughly linearly dependent on the effective water saturation. Perrier & Morat (2000) suggested a model in which the electrokinetic coefficient is dependent on a relative permeability model. Linde *et al.* (2007) and Revil *et al.* (2007) proposed a theoretical model describing the electrokinetic coefficient, based on a relative permeability model too. These two models suggest that the electrokinetic coefficient decreases with decreasing water saturation, however its dependence on water saturation was not found to be linear. Recently Jackson (2008) suggested that the electrokinetic coefficient depends on water saturation as a power law. Few experimental studies have been published on this subject. Since continuous records of the electrokinetic coefficient as a function of water saturation have not been published, to our knowledge, we developed an experimental setup which allows to acquire several independently continuous records of the streaming potential as a function of water saturation. We discuss our results in light of the previous available models and experimental data.

Unsaturated flow occurring in the vadose zone are relatively complex and depends on parameters such as water pressure, water content and hydraulic conductivity. Moreover, both the retention relation, which links water pressure to water content (Brooks & Corey 1964), and the relation between hydraulic conductivity and water content (Mualem 1976a) are strongly non-linear. The equation describing variations of these hydraulic parameters and water flow in unsaturated conditions was proposed by Richards (1931). The understanding of the hydrodynamics is essential before undertaking the study of the electrokinetic coefficient in unsaturated conditions.

In this work, several drainage experiments were performed, monitoring streaming potentials, water pressure, water content, and cumulative outflow in sand. Using the water pressure and the water-content measurements, we deduced the hydrodynamic parameters of the retention model and hydraulic conductivity model by inversion. Then the water pressure was calculated with a better signal to noise ratio than the measured one. The electrokinetic coefficient was deduced from the streaming potential measurements and from the computed total water pressures as a function of the measured water-content.

2 THEORETICAL BACKGROUND

2.1 Electrokinetic phenomena

Using near-equilibrium thermodynamics (Onsager 1931), and neglecting temperature and concentration gradients, one can write coupling relations which link both the macroscopic electrical (**J**) and hydrological (**q**) fluxes to their driving forces; the macroscopic electrical potential gradient, ∇V (V m^{-1}) and the macroscopic total water pressure gradient ∇P (Pa m^{-1}),

$$\begin{bmatrix} \mathbf{J} \\ \mathbf{q} \end{bmatrix} = \begin{bmatrix} L_{11} & L_{12} \\ L_{21} & L_{22} \end{bmatrix} \begin{bmatrix} \nabla V \\ \nabla P \end{bmatrix}. \tag{1}$$

Analysing eq. (1), the Ohm's law implies $L_{11} = \sigma_r$, with σ_r the bulk electrical conductivity (S m^{-1}). Moreover, Darcy's law implies $L_{22} = k/\eta_w$, where k (m^2) is the permeability of the medium and η_w (Pa s) the dynamic viscosity of the fluid. The streaming current associated with the driving pressure through the electrokinetic coupling, is induced by an excess of charges in the diffuse part of the EDL. The electrokinetic coupling L_{12} is related to the electrokinetic coefficient C (V Pa^{-1}) as $L_{12} = -C\sigma_r$ (A Pa^{-1} m^{-1}). If the porous medium is water saturated, C will be written as C_{sat}. Consequently, the coupled equation for the electrical current density can be written

$$\mathbf{J} = -\sigma_r \nabla V + C_{sat}\sigma_r \nabla P. \tag{2}$$

One can write the conservation of the electrical current density,

$$\nabla \cdot \mathbf{J} = -\frac{\partial \rho}{\partial t} \tag{3}$$

with ρ the surface charge density (C m^{-2}). For geological materials, one classically assume steady-state with $\partial\rho/\partial t = 0$, thus there remains only the left-hand term of eq. (2), with divergence operator $\nabla \cdot \mathbf{J} = 0$. Therefore, using eq. (2) and integrating eq. (3) in the case of a unidirectional flow through a cylindrical saturated porous capillary, one can derive the well-known Helmholtz–Smoluchowski (Smoluchowski 1905) relation of the saturated electrokinetic coefficient

$$C_{sat} = \frac{\Delta V}{\Delta P} = \frac{\epsilon_0 \epsilon_r \zeta}{\eta_w \sigma_w} \tag{4}$$

with the fluid electrical permittivity $\epsilon_0\epsilon_r$ (F m^{-1}), the fluid dynamic viscosity η_w (Pa s), the fluid electrical conductivity (S m^{-1}) and ζ (V), the zeta potential described as the electrical potential inside the EDL at the shear plane. The electrokinetic coefficient can be deduced by applying a driving pressure and by measuring the induced electrical potential. The total water pressure P (Pa) must be considered as the combination of capillary and gravity effects: $P = \rho_w g(h - z)$, where ρ_w is the density of the fluid (kg m^{-3}), g is gravity (m s^{-2}), h is the pressure head (m) and z is the elevation (m).

2.2 Unsaturated flow equations

Considering the mass conservation equation and general form of Darcy's law in 1-D leads to the mixed form of Richards equation (Richards 1931), which describes unsaturated water flow in a porous medium,

$$\frac{\partial \theta(h)}{\partial t} - \frac{\partial}{\partial z}\left[K(h)\frac{\partial h}{\partial z} - K(h)\right] = 0, \tag{5}$$

where h is the pressure head (m), K is the hydraulic conductivity (m s^{-1}) as a function of θ or h, t is time (s) and z the distance from the reference altitude (m). The vertical coordinate z is defined to be positive downward, and the reference elevation is set so that $z = 0$ corresponds to the top of the column. The symbol θ represents the volumetric water content (or moisture content) (m^3 m^{-3}).

Hydraulic conductivity and pressure head depend non-linearly on water content. The $\theta(h)$ and $K(\theta)$ relations are assumed respectively using the Brooks & Corey (1964) model,

$$Se = \frac{\theta - \theta_r}{\theta_s - \theta_r} \begin{cases} \left(\frac{h_a}{|h|}\right)^{\lambda}, & \text{if } \frac{h_a}{|h|} < 1 \\ 1, & \text{if } \frac{h_a}{|h|} > 1 \end{cases} \tag{6}$$

and the Mualem (1976a) model,

$$K(S_e) = K_s . S_e^{L+2+\frac{2}{\lambda}} \tag{7}$$

with S_e the effective water saturation defined by,

$$S_e = \frac{\theta - \theta_r}{\theta_s - \theta_r} \tag{8}$$

or by,

$$S_e = \frac{S_w - {S_w}^r}{1 - {S_w}^r}. \tag{9}$$

In eq. (6), $\theta_s = \phi$ is the water content in saturated conditions with ϕ the porosity, and θ_r is the residual water content which represents the water fraction adsorbed to the matrix grains when the medium becomes highly unsaturated. The parameter K_s is the hydraulic conductivity at saturation [m s^{-1}], S_w is the water saturation, and is linked to the water content by: $S_w = \theta/\phi$. Thus the residual adsorbed water saturation is defined as ${S_w}^r = \theta_r/\phi$. The air entry pressure is h_a [m], which characterize the threshold pressure for water content to begin to decrease during a drainage. The parameter λ is an hydrodynamic parameter depending on the pore size distribution, which classically varies from 0.9 to 3.2 for sands (Haverkamp *et al.* 1998, personal commumnication; Haverkamp *et al.* 2005; Leij *et al.* 2005). The parameter L of the eq. (7) takes into account the correlation between the pore size and flow tortuosity, it is chosen at $L = 0.5$ which is a classical value in the literature (Mualem 1976a).

Boundary conditions must be applied to Richards equation at the top and the bottom of the system. For the high and low extremity of the profile, which is a vertical 1-D cylindrical column of sand, the following boundary conditions on pressure head (Dirichlet) and flux (Neumann) can be assumed,

$$h(z,t) = h_D(t) \text{ or } \left(-K(h)\frac{\partial h}{\partial z} + K\right)_{z=0,l} = q_N(t) \tag{10}$$

with z equal to zero or l (the length of the profile). The variables $h_D(t)$ and $q_N(t)$ are respectively the imposed pressure head and net flux. A zero flux (at the top) and an imposed pressure head (at the bottom) are used as boundary conditions in the inversion process for both experiments presented in this paper.

The mixed form of the Richards equation is solved by the standard Galerkin finite element method (Pinder & Gray 1977) with a fully implicit scheme in time. The system of equations obtained is highly non-linear. To linearize the equations, the Newton method described in Lehmann & Ackerer (1998) is used.

The inverse problem is solved following a non-linear optimization process. The objective function to be minimized is defined in eq. (11). This function is the difference between measured and computed pressure head at each iteration, respectively h_i^{n+1} and $\hat{h}_i^{n+1}$, and/or water content θ_i^{n+1} and $\hat{\theta}_i^{n+1}$.

$$\mathcal{O}(\mathbf{p}) = \sum_{n=0}^{N-1}\sum_{i=1}^{N_m} w_{ih}^{n+1}\left[h_i^{n+1} - \hat{h}_i^{n+1}(\mathbf{p})\right]^2 + \sum_{n=0}^{N-1}\sum_{i=1}^{N_m} w_{i\theta}^{n+1}\left[\theta_i^{n+1} - \hat{\theta}_i{}^{n+1}(\mathbf{p})\right]^2. \tag{11}$$

The vector $\mathbf{p}$ represents adjusted parameters of the model, h_i^{n+1} and θ_i^{n+1} are the measured pressure head and water content at location i and time $n+1$ respectively. The pressure head and water content $\hat{h}_i^{n+1}$ and $\hat{\theta}_i{}^{n+1}$ are the computed model at iteration i and time $n+1$. Differences between measurements and models are computed in a least-square sense, and weight functions w_{ih} and/or $w_{i\theta}$ are also added. For more details on both forward and inverse problem process mentioned here, see Lehmann & Ackerer (1998) and Hayek *et al.* (2007). We used this approach to inverse the water pressure and the water-content measurements in order to deduce the unknown hydraulic parameters introduced by eqs (6) and (7). Hopmans *et al.* (2002) explained that pressure measurements during a drainage experiment allow a good estimation of these hydraulic parameters in the inverse approach, without knowing K_s or θ_s. In contrast, they added that these two parameters should be measured and known in the case of measuring only the cumulative water outflow without any pressure measurements. The total water pressures, ΔP are obtained from differences of water pressures, h. The uncertainty on water pressure measurements is almost 1 cm (in terms of water height) or 100 Pa. This uncertainty is too large to infer total water pressure differences (which are only 600 Pa of maximum amplitude in our case) with a good signal to noise ratio. Thus, the computed water pressures, which show a better signal to noise ratio, were used to calculate the total water pressure P. Hence, the electrokinetic coefficients were deduced from the streaming potential measurements and from computed total water pressure in Section 4.2.

2.3 Electrokinetic coefficient in unsaturated conditions

Since the electrokinetic equations were developed in saturated conditions, the effect of water content on the electrokinetic coupling is still in debate. Sprunt *et al.* (1994) showed that the streaming potential could be enhanced when bubbles are flowing within the water. It was first proposed that the electrokinetic coefficient was inversely proportional to the effective saturation with a power n, meaning that the electrokinetic coefficient decreases with increasing water saturation (Revil *et al.* 1999a; Darnet & Marquis 2004; Sailhac *et al.* 2004). Then the first experimental study on the electrokinetic coefficient behaviour in unsaturated conditions was reported by Guichet *et al.* (2003). In their work, several drainage experiments were carried out by injecting inert gas into a 1 meter long column filled with water saturated Fontainebleau sand, and streaming potentials and water content were monitored. Their study showed, contrary to predictions, that the electrokinetic coefficient linearly increases

with the effective water saturation S_e,

$$C(S_w) = C_{sat} S_e \tag{12}$$

with C_{sat}, the saturated electrokinetic coefficient.

Then Perrier & Morat (2000) suggested that the electrokinetic coefficient depends on a relative permeability model k_r,

$$C(S_w) = C_{sat} \frac{k_r}{{S_w}^n} \tag{13}$$

with k_r a relative permeability model defined as: $k_r = ((S_w - 0.1)/0.9)^2$ (Adler *et al.* 1997), and assuming that the relative electrical conductivity is equal to S_w^n. The parameter n is the Archie saturation exponent (Archie 1942), and is assumed to be 2 by Perrier & Morat (2000). This exponent has been observed to be about 2 for consolidated rocks and in the range $1.3 < n < 2$ for coarse-texture sand (Schön 1996; Guichet *et al.* 2003; Lesmes & Friedman 2006). Note that the use of Archie's law is valid in the absence of surface electrical conductivity.

Recently a new formulation including another relative permeability model was proposed by (Revil *et al.* 2007),

$$C(S_w) = C_{sat} \cdot \frac{k_r}{{S_w}^{n+1}} \tag{14}$$

assuming that the charge density of the pore space is inversely proportional to the water saturation S_w, and considering the similar behaviour of hydraulic and electrical conductivity for unsaturated conditions. The Mualem relative permeability k_r (Mualem 1976a), introduced by eq. (7), is chosen with $L = 1$ instead of $L = 0.5$.

Recently (Saunders *et al.* 2008) proposed a power law to describe the behaviour of the unsaturated relative electrokinetic coefficient during imbibition,

$$C_r(S_w) = {S_{wn}}^{n_s}. \tag{15}$$

This relation, where n_s is a positive exponent between 0.01 and 1, was used in a numerical calculation to compute downhole SP monitoring during the injection of water in oil reservoirs. This expression depends on a particular normalized water saturation given by,

$$S_{wn} = \frac{S_w - S_{wc}}{1 - S_{wc} - S_{ro}} \tag{16}$$

with S_{wc} and S_{ro}, the connate water saturation and oil saturation respectively. Eqs (15) and (16) imply the maximum of the relative electrokinetic coefficient to be around $S_w = 80$ per cent which had never been reported by experimental studies or theoretical developments up to now. In the present work, only two different phases (water and air) are considered, so that the eq. (16) would be strictly equivalent to effective water saturation, $S_{wn} = S_e$.

3 EXPERIMENTAL SETUP

Several drainage experiments in sand were performed using the experimental apparatus depicted in Fig. 1. During water flow, streaming potentials are monitored, as well as water pressure, water content, temperature and cumulative outflow. Streaming potentials are measured using 10 non-polarizable silver–silver chloride electrodes placed every 10 cm along the column. Each electrode rod is put into a porous ceramic cup (of 6 mm diameter and 28 mm length), filled with deionized water, which is in contact with the porous medium. These cups remain saturated until a pressure less than 0.1 MPa (or 1 atm) is applied, so that the cups remain electrically conducting. Therefore streaming potential measurements are still possible when the sand is unsaturated. The experimental setup consists of a 1.3 m long and 10 cm diameter plexiglass column. Each SP difference is measured between one electrode and the reference one, located at the bottom of the column. A pressure transmitter is located in the centre of each of the nine dipoles formed by each pair of consecutive electrodes. These sensors (33 and 35xx, Keller Inc.) are floating piezoresistive transducers, and measure water pressure from –0.07 to 0.07 MPa with almost 100 Pa accuracy. Moreover, water content measurements are combined to water pressure, at the same locations along the column, in order to monitor the dynamic of the water flow. Water content is measured using Theta probes ML2x (Δ-T Devices Ltd.) which are based on medium impedance measurements (Gaskin & Miller 1996). All Theta probes were calibrated using a scale-down of the column, with exactly the same geometry, using nine sand/water mixtures prepared in the whole range of water content (from 0 to θ_s with step of 0.05). Then a calibration model linking the weighted water content to the measured voltage output of the nine probes was deduced. We had also planned to measure the electrical resistivity each 10 cm along the column. Unfortunately all tests performed up to now could not allow us to deduce a correct relation which links the measured electrical resistance and the true resistivity of the medium. We measured the electrical resistivity as a function of water content by a weighting method to deduce the Archie saturation exponent n, as explained in Appendix B.

We adopt the following protocol for each drainage experiment.

(i) The column was first filled with Fontainebleau sand (Sifraco NE34) saturated with deionized water. As deionized water has a low conductivity, its conductivity increases when it is in contact with the sand. Therefore, the water was forced to circulate through the sand until its conductivity reached a constant value (reported in Table 3), so that the mixture water/sand could be considered in chemical equilibrium.

(ii) Before the drainage begins, a reservoir connected to the bottom of the column (see R1 in Fig. 1) was placed at the top level of the column. Thereby, both the sand surface and the surface of water in the reservoir represent of a free pressure surface, so that the medium is in hydrostatic state.

(iii) To start the drainage, the reservoir was moved downwards at the bottom of the column. Thus a hydraulic head difference was applied to the medium at around 1 m of water height which induces the fluid flow. After each experiment, a sample of water was collected to measure its pH and electrical conductivity.

The sand was packed as uniformly as possible, and the most heavily possible in laboratory (see Appendix A). Moreover several drainage are performed before any measurements. Unfortunately no method exists to reproduce the structure of an undisturbed soil. Packing of the column depends on the method used, on the operator and on the scale of the column (Corey 2002). During the whole experiment, until water outflow stopped, streaming potentials, water pressure and water content were recorded every 80 s using a HP34970A switch unit (Agilent Technologies) coupled with a HP34901a multiplexer module, remotely controlled by a computer. This unit provides a internal impedance greater than 10 GΩ. Electrical potential differences were also integrated on 100 periods of the 50 Hz signal, so that each measurement was performed over 2 s. This averaging allows the automatic rejection of the 50 Hz anthropogenic electrical noise. We detailed in Appendix A the tests that we performed to ensure that we have measured correctly the streaming potentials. In the next part we will present all the signals measured as a function of time. In addition, petrophysical characteristics of the sand are reported in Table 1. We discuss in this paper two experiments: the first one lasted about 200 hr, and the second one 300 hr. These

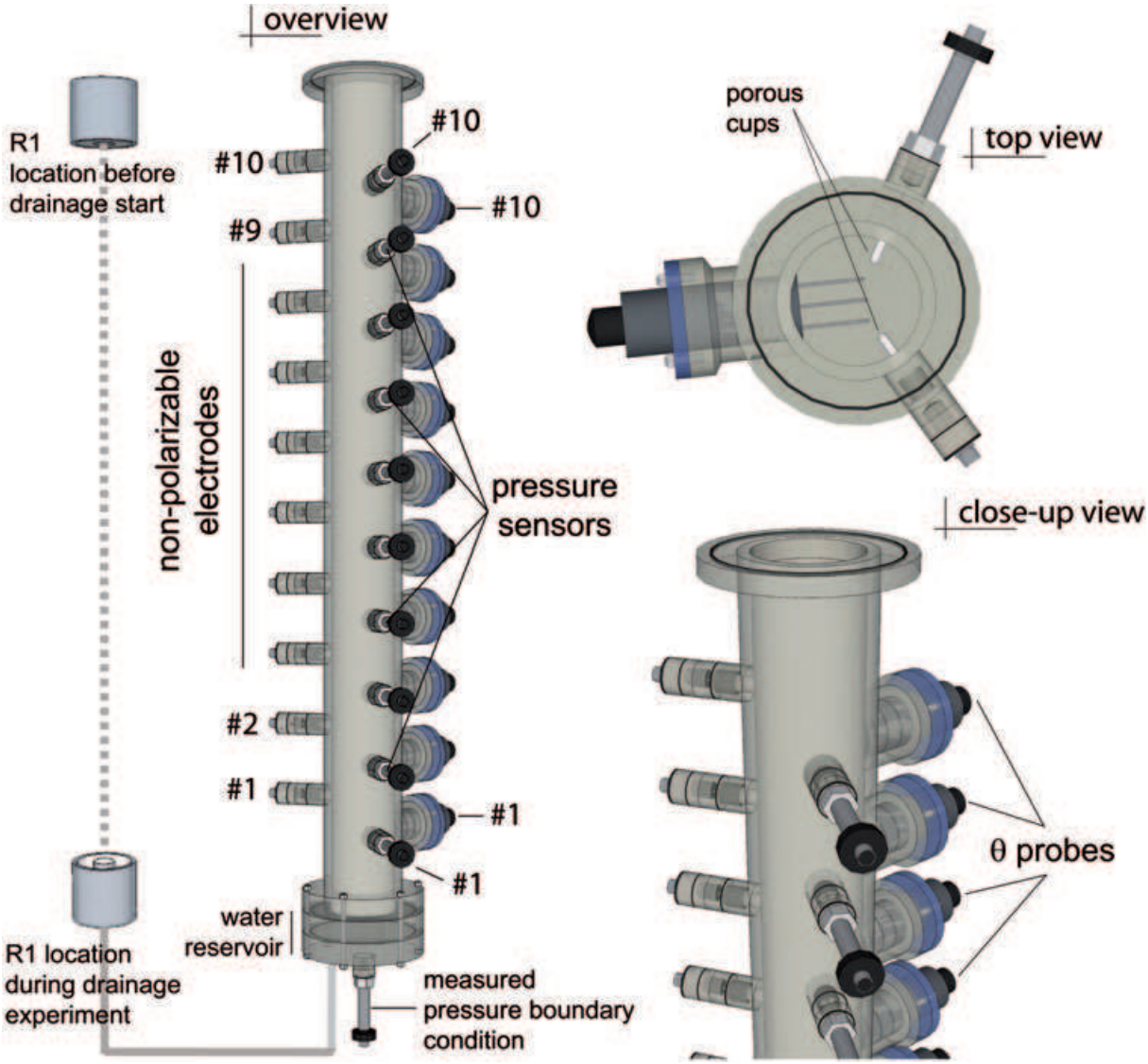

Figure 1. Sketch of the experimental setup. The plexiglas column is 10 cm diameter and 1.3 m height. Ten non-polarizable electrodes are located every 10 cm along the column. The water reservoir R1 is used to apply the pressure condition at the bottom of the column. A pressure sensor monitors this boundary condition during the experiment.

Table 1. Petrophysical characteristics of the sand.

ϕ (–)	Grains size (μm)	q_{25}, q_{60}, q_{75} (μm)	SiO_2 (per cent)	Others components (per cent)
0.36–0.37	100–300	247, 220, 165	>99.7	<0.3

experiments allowed us to obtain independently seven continuous records for the behaviour of the electrokinetic coefficient versus water saturation.

4 EXPERIMENTAL RESULTS

4.1 Hydrodynamic measurements

Water pressures and water-content measurements were used to estimate the hydraulic parameters of the sand K_s, h_a, λ, θ_s and θ_r using the numerical scheme described in Section 2 (eqs 6 and 7). Before drainage starts ($t \simeq 20$ hr), when the medium is still in hydrostatic equilibrium, a 10 cm pressure head shift between each sensor is observed (see Fig. 2a). The dashed and solid lines are the results of the inversion process and fit the measured water pressure head quite well. Measured water saturations begin to decrease one after the other during the drainage, as time progresses (see Fig. 2b). This time shift is related to the air entry pressure, defined as h_a, so that a pressure head around -40 cm is required before the water content begins to decrease. The time axis should be interpreted as representing the direction of decreasing water saturation. Thus, curves in Fig. 2(b) characterize the water front propagation within the column, and consequently informs us about the flow dynamics of the experiment. Estimated values for K_s, h_a, λ, θ_s and θ_r are reported in Table 2. Measured value of K_s is also reported in

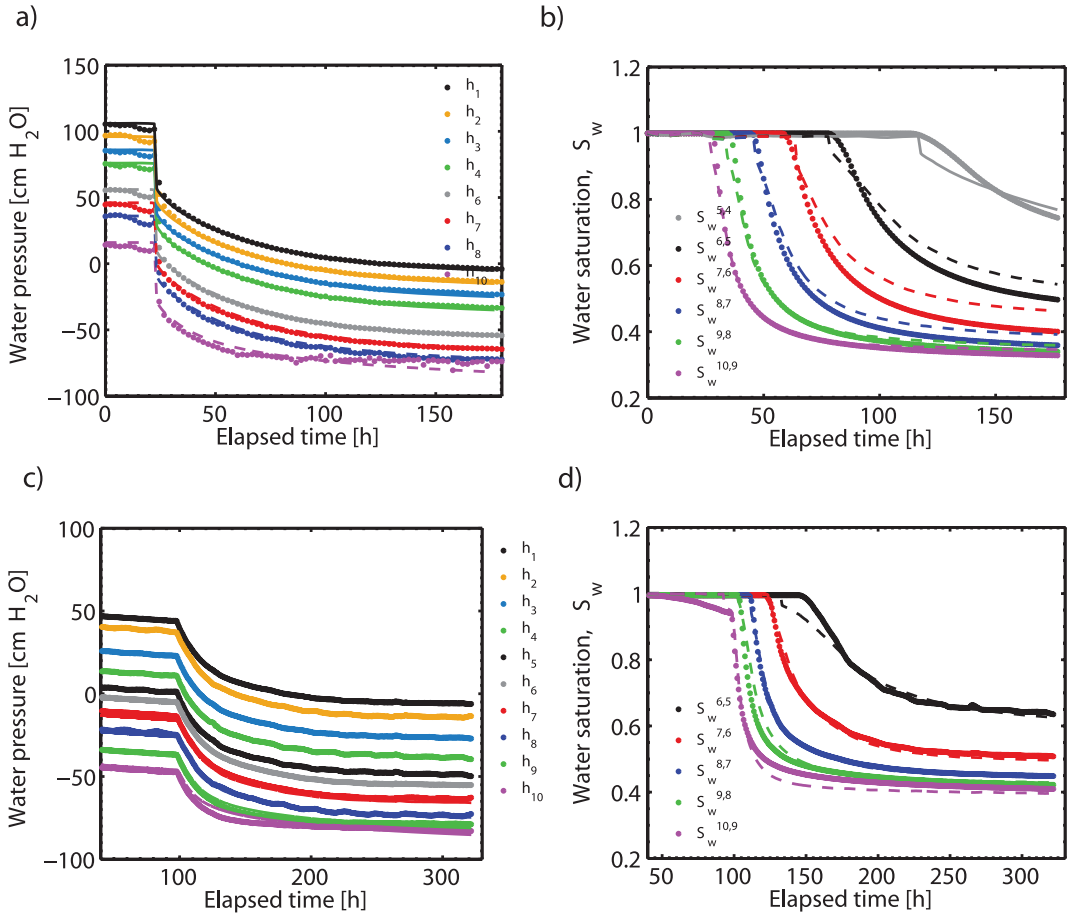

Figure 2. Measured (dots) and computed (lines) water pressure head (expressed in water height) for experiment #1 (a) and experiment #2 (c). Indice #1 of h_1 indicates the measurement at the bottom and indice #10 the one at the top of the column. Measured (dots) and computed (lines) water saturation for experiment #1 (b) and experiment #2 (d). Exponent i of each $S_w{}^i$ indicates the location of the θ probe inside the column. Drainage started at 22 hr for experiment #1 and 95 hr for experiment #2.

Table 2. Hydrodynamic parameters values deduced from the inversion process.

Experiment	K_s ($\times 10^{-5}$) (m s^{-1})	K_s^{meas} ($\times 10^{-5}$) (m s^{-1})	h_a (m)	λ	θ_r	θ_s (m^3 m^{-3})	$S_w{}^r$ (–)
1	1.65	17.2	0.4	3.88	0.11	0.355	0.305
2	2.72	17.2	0.45	3.65	0.12	0.358	0.33

Notes: The $S_w{}^r$ values are deduced from θ_r through $S_w{}^r = \theta_r/\phi$. The K_s^{meas} is the measured permeability of our sand. The saturation Archie exponent is measured $n = 1.45$.

Table 2. It is slightly greater than the computed K_s considering that the permeability range is over 22 orders of magnitude, and still in the classical range for sandy texture soils (Carsel & Parrish 1988). Using measured value or inverted value of K_s lead to the same results for the calculated pressures during the drainage experiments, and fit the measured pressures. The results are in good agreement with classical values in the literature for this kind of medium (Rawls *et al.* 1982). Figs 2(c) and (d) show the results for the second experiment. The similarity of the estimated values of K_s, h_a and λ let us conclude that the two experiments are very similar in terms of hydrodynamics. The estimated values of λ are significantly higher than values introduced in Section 2.2. Using the technical specifications of the sand, we can compute the Trask (or sorting) index S_o and the Hazen (or uniformity) coefficient C_u (Rivière 1977). This calculation requires the quantile q_{25}, q_{60} and q_{75} of the granulometric curve, and gives information on granulometric caracteristics of the sand. We found $S_o = 1.22$ and $C_u = 1.46$ demonstrating that the grain size is very well sorted (monodisperse), resulting in relatively high values of λ.

4.2 Electrokinetic measurements

Streaming potentials are measured between one electrode and the reference (electrode #1, see Fig. 1). As for water-content measurements, a time-shift is observed between the beginning of the decrease of each record. Water content measurements were assumed to be integrated over a volume delimited by two consecutive non-polarized electrodes forming a dipole because each water content probe is located in the middle of a dipole. Thus the entire column can be divided into nine different horizontal layers 10 cm high, in which measured streaming potential, measured and computed total water pressure differences and measured water saturations are known as a function of time. Streaming potential differences for each dipole were inferred from the raw measurements, for the top-five layers

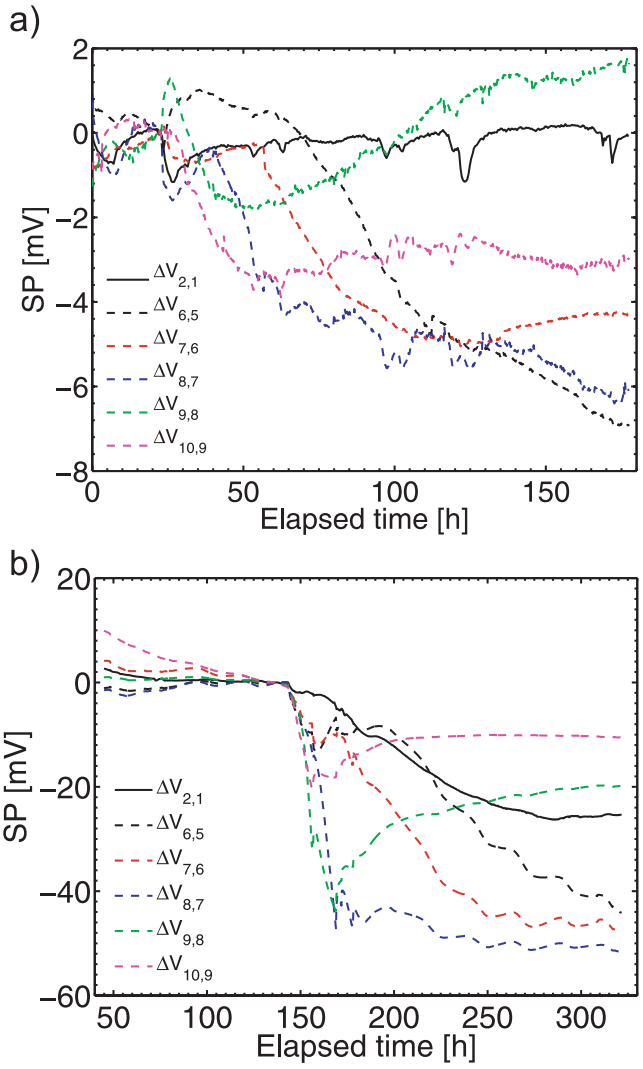

Figure 3. The streaming potentials signals for several dipoles during the drainage for experiment #1 (a) and experiment #2 (b). The SP differences at the beginning are zero, because the voltage shift before the experiment was cancelled. Indices indicate the location of dipoles: $\Delta V_{10,9}$ is SP between electrodes #10 and #9 (see Fig. 1). The dashed lines are the dipoles located in the unsaturated part of the sand at the end of the drainage. The dipole $\Delta V_{2,1}$ (solid black line) is always located in the saturated part. Drainage started at 22 and 95 hr for experiments #1 and #2, respectively.

in the column. The maximum absolute value of streaming potential is around 7 mV for the first experiment, and almost 45 mV at the end of the second experiment (see Fig. 3). Consequently, signals of the first experiment (Fig. 3a) are slightly more noisy than those of the second one (Fig. 3b). The streaming potential absolute values increase during the drainage, when the water saturation decreases.

We need the total water pressure differences in order to compute the electrokinetic coefficient for each layer inside the column. Total water pressure differences (Fig. 4) are inferred for each layer from computed water pressures. Since we showed that the computed values fit the measured values well (Fig. 2), computed values of water pressure were preferred over the measured water pressures. The drainage start is characterized by a jump of the computed ΔP. This jump is about 60 Pa for both experiments. After several hours, ΔP inside the layers in the unsaturated part of the column increases. The maximum of ΔP at the end of the experiment depends on the saturation degree in the considered layer; the lower the saturation degree, the higher the ΔP. Thus, $\Delta P_{10,9} \simeq 550$ Pa and $\Delta P_{9,8} \simeq 450$ Pa for the first experiment. Computed ΔP corresponding to layers always located in the saturated part of the column (Fig. 4) progressively decrease from the start jump to zero.

Using measured streaming potential and computed total water pressure, the following equation leads to electrokinetic coefficient,

$$C = \frac{\Delta V}{\Delta P}. \tag{17}$$

Electrokinetic coefficients were computed only in the four layers located in the unsaturated part of the column, that is, $C_{10,9}$, $C_{9,8}$, $C_{8,7}$ and $C_{7,6}$ for the first experiment, and for $C_{10,9}$, $C_{9,8}$, $C_{8,7}$ for the second one. The data from other dipoles (i.e. $C_{6,5}$ and lower for exp. 1, and $C_{7,6}$ and lower for exp. 2) were not used because the small values of ΔP gave an unacceptable signal to noise ratio. The electrokinetic coefficient at saturation was measured during another experiment, and the electrical resistivity was measured at various water contents (see Appendix B).

Obtained values of electrokinetic coefficient are all negative, which involves a negative zeta potential, as expected in sand (Pride & Morgan 1991; Lorne *et al.* 1999a). The water electrical conductivity and the minimum values of the electrokinetic coefficient observed in each horizontal layer are given in Table 3. These electrokinetic coefficient maximum values (in absolute value) are higher than measured values for similar water conductivities (Ishido & Mizutani 1981; Lorne *et al.* 1999a) (Fig. B1b).

Classically, the minimum value (i.e. greatest negative value) of the electrokinetic coefficient is identified in saturated conditions. Measurements of $C_{\rm sat}$ performed on our sand are presented in Appendix B (Fig. B1). The values of $C_{\rm sat}$ corresponding to water salinities of experiments #1 and #2 are reported in Table 3. First, the electrokinetic coefficients appear to be not monotonously dependent on water saturation during our drainage experiments (i.e. when water saturation decreases) (Fig. 5). Second, it is clear that the extremum value of the electrokinetic coefficient $C_{\rm min}$, regardless of the considered dipole, is much greater than the $C_{\rm sat}$ (in absolute value). We also point out that the signals of the first experiment are scattered at the drainage start as shown by a statistical analysis on the uncertainty of the un-normalized measurements (Fig. B3). This is why the small values near zero can be either small negative values or small positive values.

5 DISCUSSION

We found the electrokinetic coefficients for unsaturated conditions to increase for decreasing water-saturation between 100 and 65–80 per cent. The coefficients for unsaturated conditions exceed the coefficient at saturation by a factor of 10–200 (Fig. 6). Our measurements are the first continuous records of the variation in electrokinetic coefficient with water-saturation; thus the proposed power laws (eqs 19 and 25) that fit the data are not expected to explain the underlying physics but more simply to provide a first basis for empirical models. Current models do not predict but fail to explain this behaviour. Only the observed decrease in electrokinetic coefficient with water-saturation below about 0.65–0.8 can be addressed by current models as will be shown below. The exact physical meaning of the observed increase in electrokinetic coefficient with decreasing saturation is not yet understood. Recently, Jackson (2010) suggested that the relative electrokinetic coefficient $C_{\rm r} = C(S_{\rm e})/C_{\rm sat}$ could be larger than one, but still considerably lower than found in our measurements. Jackson (2010) proposed

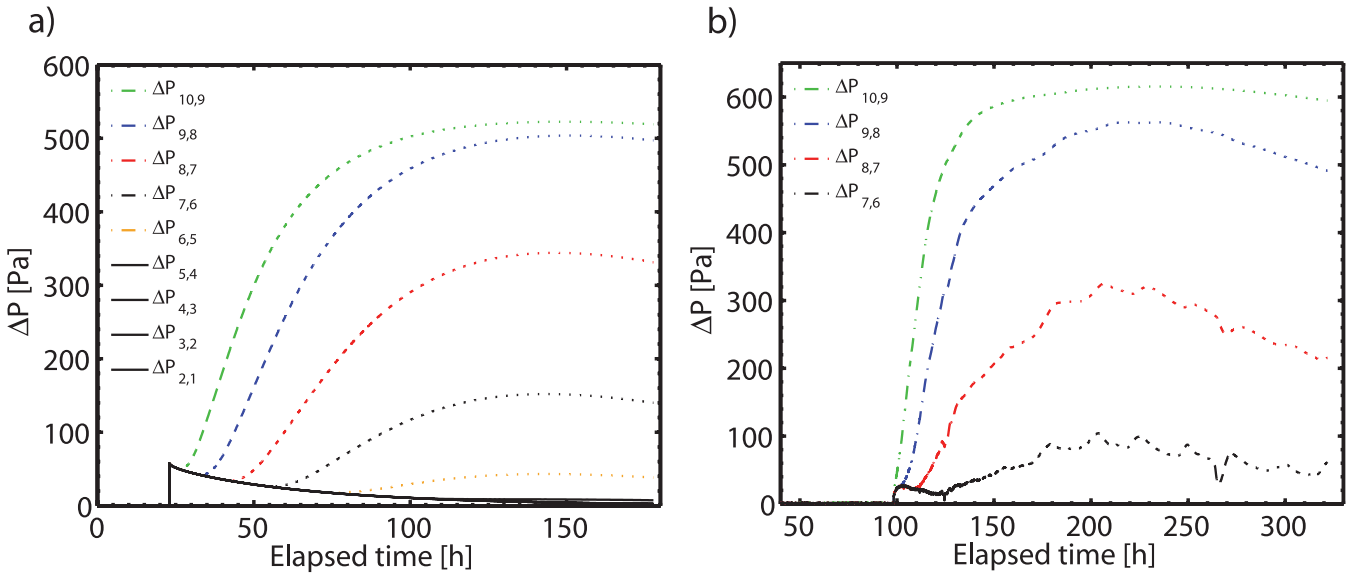

Figure 4. The computed total water pressure (Pa), deduced from computed water pressures using $\Delta P = \rho_w g(h - z)$, for (a) experiment #1 and (b) experiment #2. The dashed lines identify the layers located in the unsaturated sand at the end of the drainage. The black lines identify the layers always located in the saturated part (these lines are mixed up).

Table 3. Minimum values of C(S_w) in the unsaturated layers and saturated values C_{sat}.

Exp #1		Exp #2	
Dipole	C_{min} (V Pa^{-1})	Dipole	C_{min} (V Pa^{-1})
10, 9	-1.67×10^{-5}	10, 9	-6.7×10^{-5}
9, 8	-2.04×10^{-5}	9, 8	-2.7×10^{-4}
8, 7	-4.8×10^{-5}	8, 7	-5.9×10^{-4}
7, 6	-5.3×10^{-5}	/	/
$\sigma_w(\times 10^{-4})$ (S m^{-1})		$\sigma_w(\times 10^{-4})$ (S m^{-1})	
103.2		66.4	
C_{sat} (V Pa^{-1})		C_{sat} (V Pa^{-1})	
-1.6×10^{-6}		-2.5×10^{-6}	

Notes: The water electrical conductivity was measured at the end of each drainage. The equilibrium phase is detailed in Appendix A.

that the increase in C_r with decreasing water saturation was linked to the fraction of small capillaries in the medium. However, a direct comparison with Jackson's model for water/oil imbibition is not possible since our experiment represent drainage of water from sand.

The electrokinetic coefficient is normalized to its extremum value, which is usually observed at saturation. Since we observed an extremum around 70 per cent of saturation we also normalized the electrokinetic coefficient by the minimum value observed during each drainage C_{min} (Fig. 7) computed through:

$$C_{norm} = \frac{C(S_w)}{C_{min}}. \quad (18)$$

The comparison between our results and the current models (normalized to an extremum value at saturation, C_{sat}), could help the interpretation of the electrokinetic coefficient behaviour at saturations below our observed extremum value, meaning below about 70 per cent of saturation. In addition to our data set, the experimental results of Guichet *et al.* (2003), performed on sand, are also reported (Fig. 7). This comparison shows some consistency of our measurements normalized to the minimum value with existing published values of relative coefficient C_r (normalized to C_{sat}). As the electrokinetic coefficient values are negative, the normalization by its minimum implies positive values. During the first experiment, when S_w decreases from 1 to 0.8, C_{norm} in the four unsaturated layers increases. Then, for ${S_w}^{min} < S_w < 0.8$, C_{norm} monotonously decreases. The parameter ${S_w}^{min}$ is introduced here to characterize the minimum of the measured water saturation. It is preferred to ${S_w}^r$, since ${S_w}^r$ is a parameter which clearly depends on experimental conditions, like applied ΔP or temperature for instance. Thus, in the conditions of our experiments, there was no flow for $S_w < 0.35 (\equiv S_e < 0.08)$ and for $S_w < 0.4 (\equiv S_e < 0.11)$ for the first and the second drainage respectively. For the second experiment (Fig. 7b), C_{norm} increases when S_w decreases from 1 to about 0.95 considering the dipole (8, 7) and from 1 to 0.8 for the dipole (9, 8). The value of C_{norm} for the dipole (10, 9) is maximum when S_w is around 0.65. The slope of the increasing part of this signal (for $0.55 < S_w < 1$) is smaller than for the two other dipoles. Therefore, a shift from $\simeq$15 to $\simeq$20 per cent (for $C_{10,9}$ of exp. #2) of the maximum location is observed between the two experiments, however both experiments describe a similar behaviour of $C(S_w)$ in the whole range of water saturation. Thus, one can conclude that the electrokinetic coefficient does not depend monotonously on the water-content, either linearly nor as a power law, as suggested by previous studies. The maximum of the normalized electrokinetic coefficient is located between 0.65 and 0.95 of water saturation. This complex behaviour of the electrokinetic coefficient has never before been reported, especially the large increase for $0.8-0.95 < S_w < 1$ (excluding $C_{10,9}$ of the second experiment), and is a very important result for the understanding of electrokinetic phenomena in unsaturated media.

We compare our measurements, normalized using eq. (18), to the four C_r models introduced in Section 2 (normalized to the value at saturation) by eqs (12), (13) and (15) (Fig. 8). Hydraulic parameter λ deduced from our modelling of water-flow (Table 2) and $L = 0.5$ were used in eq. (7), to compute eq. (14). In addition, a modified model from Perrier & Morat (2000) is also computed using ${S_w}^r$ from the inversion process, instead of the value 0.1 for ${S_w}^r$ they used in their k_r model (eq. 13). Furthermore, the saturation Archie exponent n needed to compute these models is deduced from electrical resistivity measurements carried out on a small-scale column (used

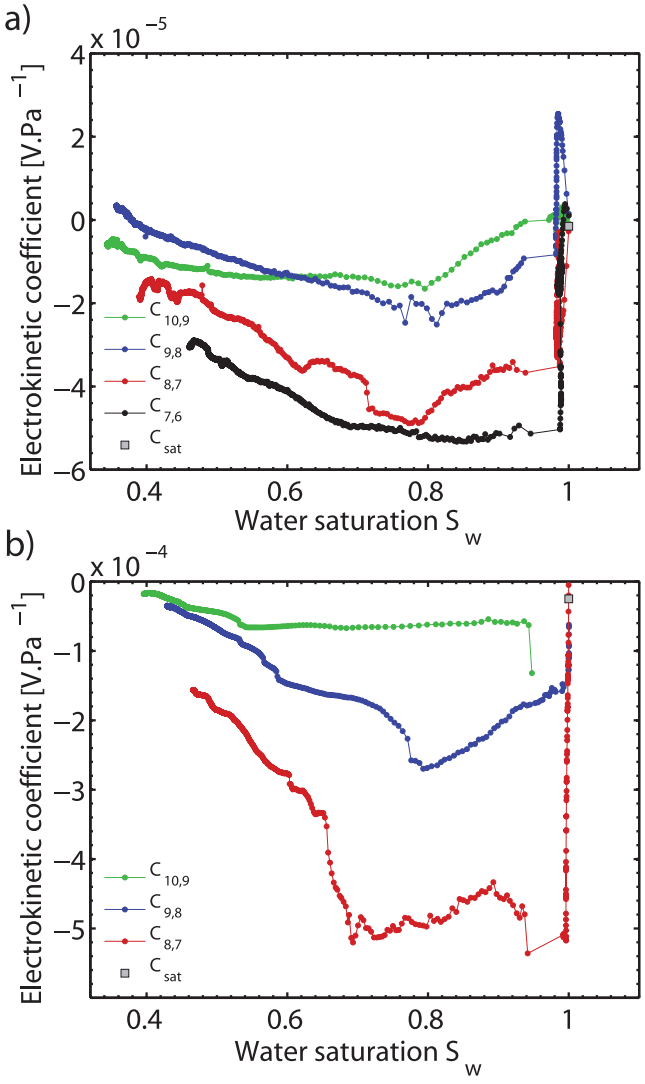

Figure 5. Raw (i.e. non-normalized) electrokinetic coefficient for experiment #1 (a), and for experiment #2 (b). The grey square is the measured C_{sat} (see Appendix B for details). It is equal to -1.6×10^{-6} V Pa^{-1} for experiment #1 and to -2.5×10^{-6} V Pa^{-1} for experiment #2.

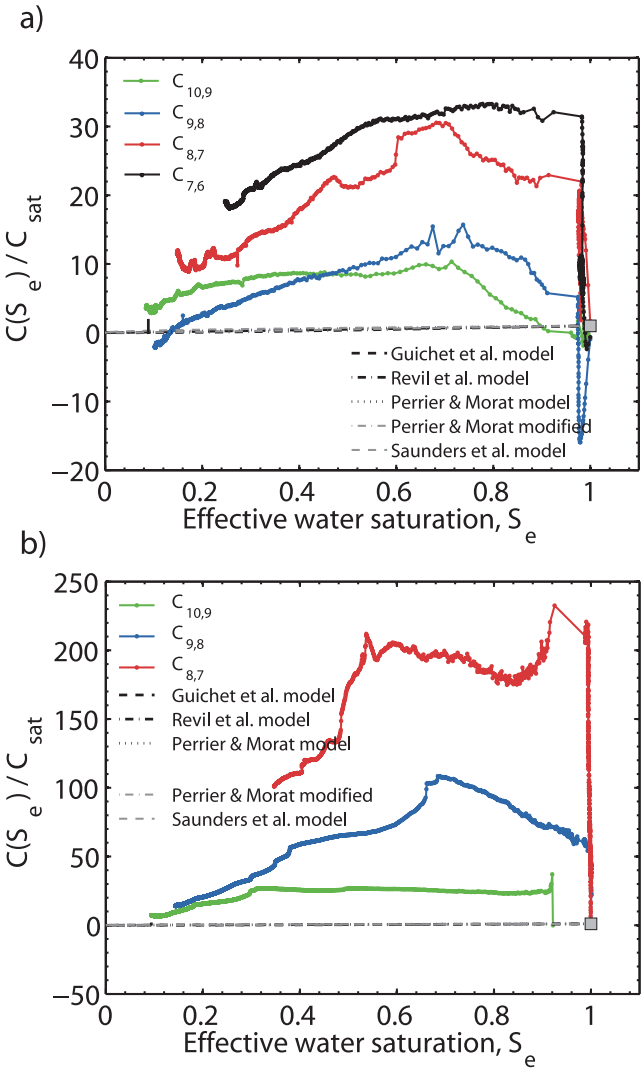

Figure 6. The relative electrokinetic coefficient computed with C_{sat} reported in Table 3, for experiment #1 (a) and experiment #2 (b). The absolute value of C_{min} is one to two orders of magnitude larger than C_{sat} and implies large maximum values of C_r. The Guichet *et al.* (2003), Perrier & Morat (2000) and Revil *et al.* (2007) models are also reported using parameters of Table 2 ($n = 1.45$ was measured, see Appendix B), and Saunders *et al.* (2008) model is computed for $n_s = 0.5$.

for Theta probe calibration), and its value is $n = 1.45$ (see Appendix B for details). These models describe a uniform decrease of the normalized electrokinetic coefficient as water saturation decreases. Moreover, their common feature is that C_{sat} is the maximum value of the electrokinetic coefficient. Although these models depend on a combination of S_e or S_w, we compared them to a power law of the effective water saturation. The Guichet *et al.* (2003), Saunders *et al.* (2008) and the Perrier & Morat (2000) models show a convex curvature. Comparing these three models to a law of the form ${S_e}^{\beta}$ leads to β equal to 1, 0.5 and $\simeq$0.8, respectively. By contrast, the Revil *et al.* (2007) and the modified Perrier & Morat (2000) models show a concave curvature. The same comparison to a power law would lead to exponents around 1.55 and 1.2, respectively. It seems that our data set, when ${S_e}^{min} < S_e < 1$, would be better fitted by a model with a convex curvature, which corresponds to an exponent β less or close to 1. One can conclude that our data set cannot be explained by existing models in the whole range of saturation, because of the presence of two different behaviours of the electrokinetic coefficient, in two water saturation domains.

In order to model the behaviours of C_{norm} for ${S_e}^{min} < S_e < 0.7$–0.9 and for 0.7–$0.9 < S_e < 1$, we propose to fit our measurements by an empirical law introduced by eq. (19). These two domains exclude the dipole $C_{10,9}$ of the second experiment (with the maximum value of C_{norm} located at $S_e = 0.55$), which will be considered apart.

$$\frac{C(S_w)}{C_{min}} = \alpha \left(\frac{\theta - \theta_r}{\theta_s - \theta_r} \right)^{\beta} = \alpha {S_e}^{\beta}, \qquad (19)$$

where α and β are adjusted parameters (–) and S_e is the effective water saturation. This empirical law, based on our continuous records, is an alternative law which can be used when the behaviour of the electrokinetic coefficient as a function of water saturation is necessary. The eq. (19) was fitted (Fig. 9) in a least-square sense to electrokinetic coefficient data. A constraint was used to force $\max(C_{norm}) \simeq 1$, within a tolerance of 10 per cent. The fit of eq. (19) was performed independently for ${S_e}^{min} < S_e < 0.7$–0.9 and for 0.7–$0.9 < S_e < 1$, except for the dipole $C^2_{10,9}$ for which the

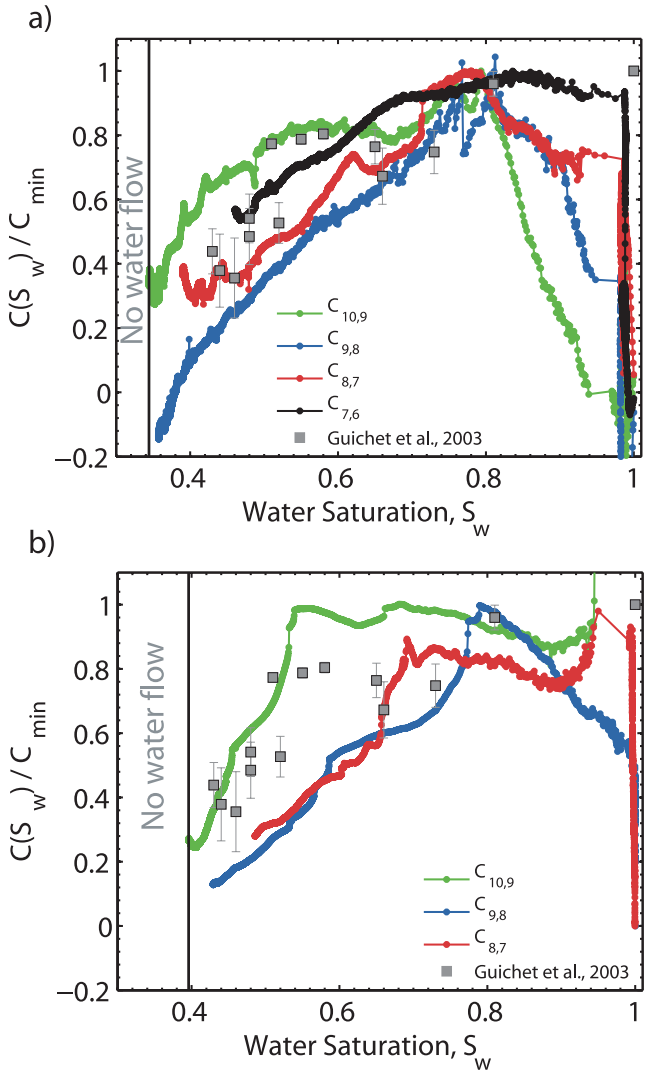

Figure 7. The electrokinetic coefficient deduced from measured SP data and computed total water pressures for experiment #1 (a) and experiment #2 (b). These values are normalized to the minimum value (eq. 18). The grey squares are experimental data on sand from Guichet *et al.* (2003), normalized to C_{sat}.

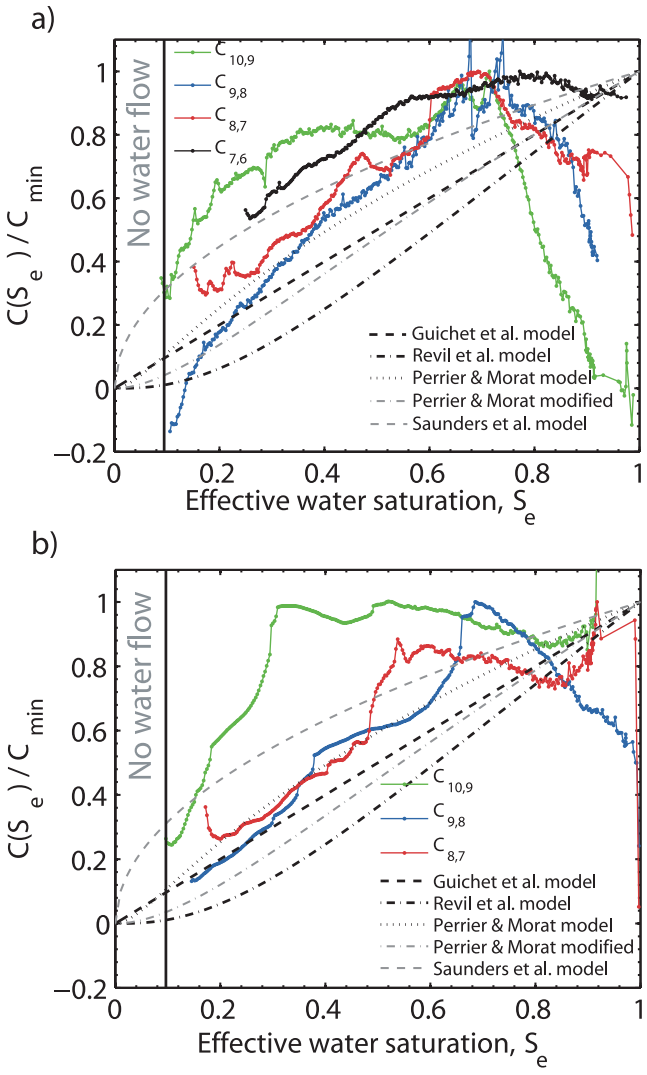

Figure 8. The electrokinetic coefficient deduced from our measurements, normalized to the minimum value, for experiment #1 (a) and experiment #2 (b). The Guichet *et al.* (2003), Perrier & Morat (2000) and Revil *et al.* (2007) models of $C_r(S_e)$ (i.e. normalized to C_{sat}) are computed using parameters of Table 2, and Saunders *et al.* (2008) model is computed with $n_s = 0.5$.

equation was fitted for ${S_e}^{min} < S_e < 0.55$, $0.55 < S_e < 0.9$ and in the whole saturation domain (${S_e}^{min} < S_e < 0.9$). The dipole $C_{8,7}$ of the second experiment was not fitted for $0.9 < S_e < 1$, because less than ten points were available in this part where water saturation decreases very fast. We first consider all the dipoles except $C_{10,9}$ for the second experiment. Computed values of α and β are reported in Table 4. These values show that a power law from ${S_e}^{0.32}$ to ${S_e}^{1.22}$ for ${S_e}^{min} < S_e < 0.7-0.9$ fits the data, depending on the chosen dipole (Fig. 9). Saunders *et al.* (2008) suggested that this exponent could vary between 0.01 and 1, which is consistent with our results in the domain ${S_e}^{min} < S_e < 0.55-0.9$. The fit of the eq. (19) in the range $0.7-0.85 < S_e < 1$ leads to negative values of β. We deduce that β can varies from -8.5 to -0.58. The dipole $C_{10,9}$ of the second experiment shows some different behaviour, so that exponent β was adjusted three times, for ${S_e}^{min} < S_e < 0.55$, for $0.55 < S_e < 0.9$ and in the whole range of saturation. Adjusted values of β are then 0.65, -0.26 and 0.25, respectively. Thus, the widest range of β would be from -8.5 to -0.26 for $0.55-0.9 < S_e < 1$ and from 0.32 to 1.22 for ${S_e}^{min} < S_e < 0.55-0.9$. Moreover, we can conclude that the exponent β is less or very close to 1. Thus, an empirical law based on all signals, is here proposed to characterize the behaviour of the electrokinetic coefficient in unsaturated conditions:

$$C_{norm} = \alpha {S_e}^{\beta}$$

$$\text{with} \begin{cases} -8.5 < \beta < -0.26, & \text{for } 0.55 - 0.9 < S_e < 1 \\ 0.32 < \beta < 1.22, & \text{for } {S_e}^{min} < S_e < 0.55 - 0.9. \end{cases} \quad (20)$$

The $C^1_{10,9}$ signal shows a distinct maximum as a function of saturation (see Fig. 9a), whereas the one for $C^2_{10,9}$ is less marked. However, the dipole (10, 9) seems to have a particular behaviour in both experiments compared to other dipoles in terms of fitted β, so that it will be considered independently in the next part of this work.

We concluded previously that both Perrier & Morat (2000) and Revil *et al.* (2007) models could not fit our measurements using the eqs (13) and (14). We propose to modify these two relations by introducing a new parameter that we can call the electrokinetic residual

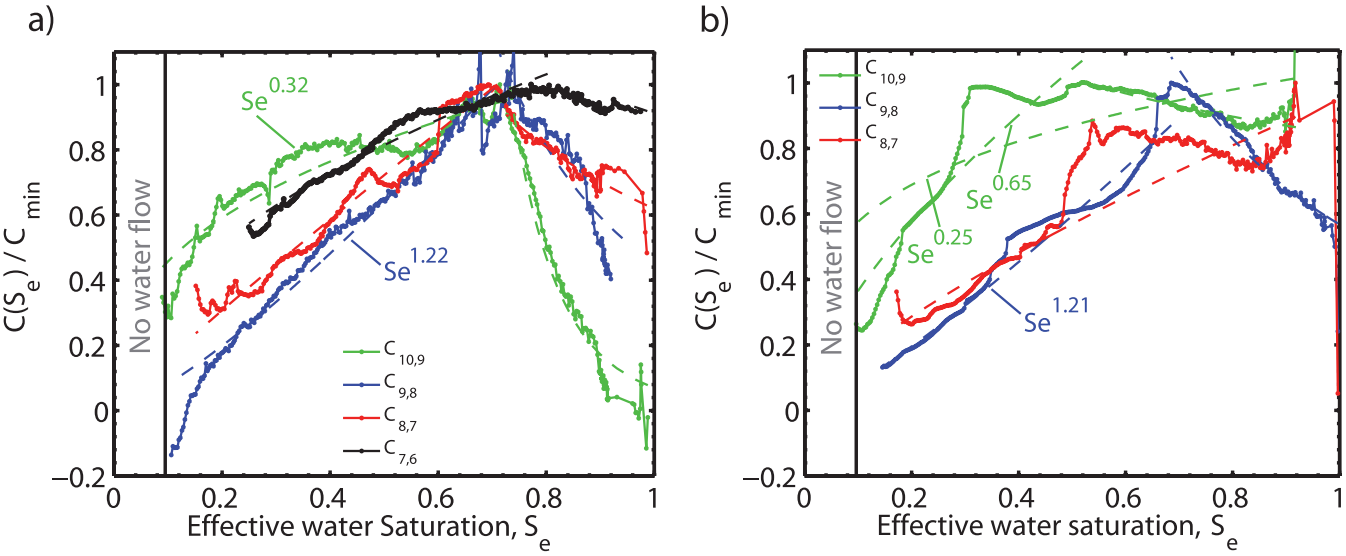

Figure 9. The electrokinetic coefficient deduced from our measurements, normalized to the minimum value, for experiment #1 (a) and experiment #2 (b). The results of least-square adjustments using eq. (19) are represented with dashed lines.

Table 4. Fitted parameters of eq. (19) in decreasing and increasing phase of the electrokinetic coefficient.

	$S^{\min} < S_e < 0.7-0.85$		$0.7-0.85 < S_e < 1$	
Dipole	α [–]	β [–]	α [–]	β [–]
$C^1_{10,9}$	1.04	0.32	0.07	−8.5
$C^1_{9,8}$	1.51	1.22	0.45	−2.6
$C^1_{8,7}$	1.42	0.97	0.62	−1.19
$C^1_{7,6}$	1.14	0.49	0.91	−0.58
$C^2_{10,9}$	1.64	0.65	0.85	−0.26
$C^2_{9,8}$	1.38	1.21	0.56	−1.69
$C^2_{8,7}$	0.96	0.75	/	/
	$S^{\min} < S_e < 0.9$			
$C^2_{10,9}$	0.26			

Note: Exponents 1 and 2 mean first and second experiment, respectively.

saturation, written $S_w^{r,ek}$. This parameter corresponds to the water saturation at which electrokinetic coupling stops. We consider that the residual water saturation $S_w{}^r$, classically used in hydrodynamics to characterize the volume of adsorbed water in unsaturated conditions, is different from $S_w^{r,ek}$. Using this concept, let us write again two relations based on eqs (13) and (14) to describe the normalized electrokinetic coefficient

$$C_{\text{norm},1} = \frac{\Gamma_{w,1}}{S_w{}^n} \tag{21}$$

$$C_{\text{norm},2} = \frac{\Gamma_{w,2}}{S_w{}^{n+1}}, \tag{22}$$

where $\Gamma_{w,1}$ and $\Gamma_{w,2}$ are deduced by analogy to relative permeability models. $\Gamma_{w,1}$ is defined by,

$$\Gamma_{w,1} = \left(\frac{S_e - S_w^{r,ek}}{1 - S_w^{r,ek}}\right)^2 = S_{ek}{}^2 \tag{23}$$

and $\Gamma_{w,2}$ by,

$$\Gamma_{w,2} = \left(\frac{S_e - S_w^{r,ek}}{1 - S_w^{r,ek}}\right)^{L+2+\frac{2}{\lambda}} = S_{ek}{}^{L+2+\frac{2}{\lambda}} \tag{24}$$

with S_{ek} the electrokinetic water saturation. The functions $\Gamma_{w,1}$ and $\Gamma_{w,2}$ are very close to those in Adler *et al.* (1997) and Mualem (1976a), respectively. We also propose the following relationship, which is modified from the eq. (19),

$$C_{\text{norm}} = \left(\frac{S_e - S_w^{r,ek}}{1 - S_w^{r,ek}}\right)^{\beta_{ek}} = S_{ek}{}^{\beta_{ek}}. \tag{25}$$

We used eqs (21), (22) and (25) to fit four electrokinetic coefficient curves from the two experiments presented in this work, $C^1_{9,8}$, $C^1_{8,7}$, $C^2_{9,8}$ and $C^2_{8,7}$. These relations are fitted in a least-square sense with $S_w^{r,ek}$ adjusted but constrained to be positive. The parameter β_{ek} of the eq. (25) is also adjusted. The results of this calculation are shown in Figs 10(b), (d) and (f). As it was noticed before, the dipoles $C^1_{10,9}$ and $C^2_{10,9}$ were considered independently (Figs 10a,c and e). In the same way than for eq. (19), the eqs (21), (22) and (25) were fitted to $C^2_{10,9}$ in the whole range of saturation, and for $S_e{}^{\min} < S_e < 0.55$ independently. The values of $S_w^{r,ek}$ (Table 5) are smaller than $S_w{}^r$ values (Table 2). The fitted $S_w^{r,ek}$ from eqs (21) and (22) are very similar only for a given dipole. These two models are extremely dependent on the chosen $\Gamma_{w,i}$ (particularly on the power exponent) and on Archie's saturation exponent n, which is involved in the behaviour of the unsaturated electrical conductivity. Indeed, the numerator and the denominator exponents balance each other. These models are roughly equivalent, leading to similar values of $S_w{}^{r,ek}$. Moreover, these two models seem to have not enough degrees of freedom to fit data from dipoles $C^1_{10,9}$ and $C^2_{10,9}$. The third model fit (equation 25) gives some higher and very homogeneous values of $S_w^{r,ek}$, around 0.13 for dipoles $C^1_{9,8}$, $C^1_{8,7}$, $C^2_{9,8}$ and $C^2_{8,7}$, and around 0.09 for dipoles $C^1_{10,9}$ and $C^2_{10,9}$. Values of β_{ek} are also very homogeneous from a dipole to another. The results gives $\beta_{ek} \simeq 0.2$ for $C^1_{10,9}$ and $C^2_{10,9}$, and $0.4 < \beta_{ek} < 0.6$ for $C^1_{9,8}$, $C^1_{8,7}$, $C^2_{9,8}$ and $C^2_{8,7}$. These coherent values for both parameters $S_w^{r,ek}$ and β_{ek} lead to the conclusion that the model we propose through eq. (25) is more appropriate than the models given by eqs (21) and (22).

In order to roughly estimate the thickness of the adsorbed water layer corresponding to the electrokinetic residual saturation, we propose to use the method described by Knight (1991) to compute the equivalent number of monolayers of water. This method uses the assumption that all the water is present as a layer with constant

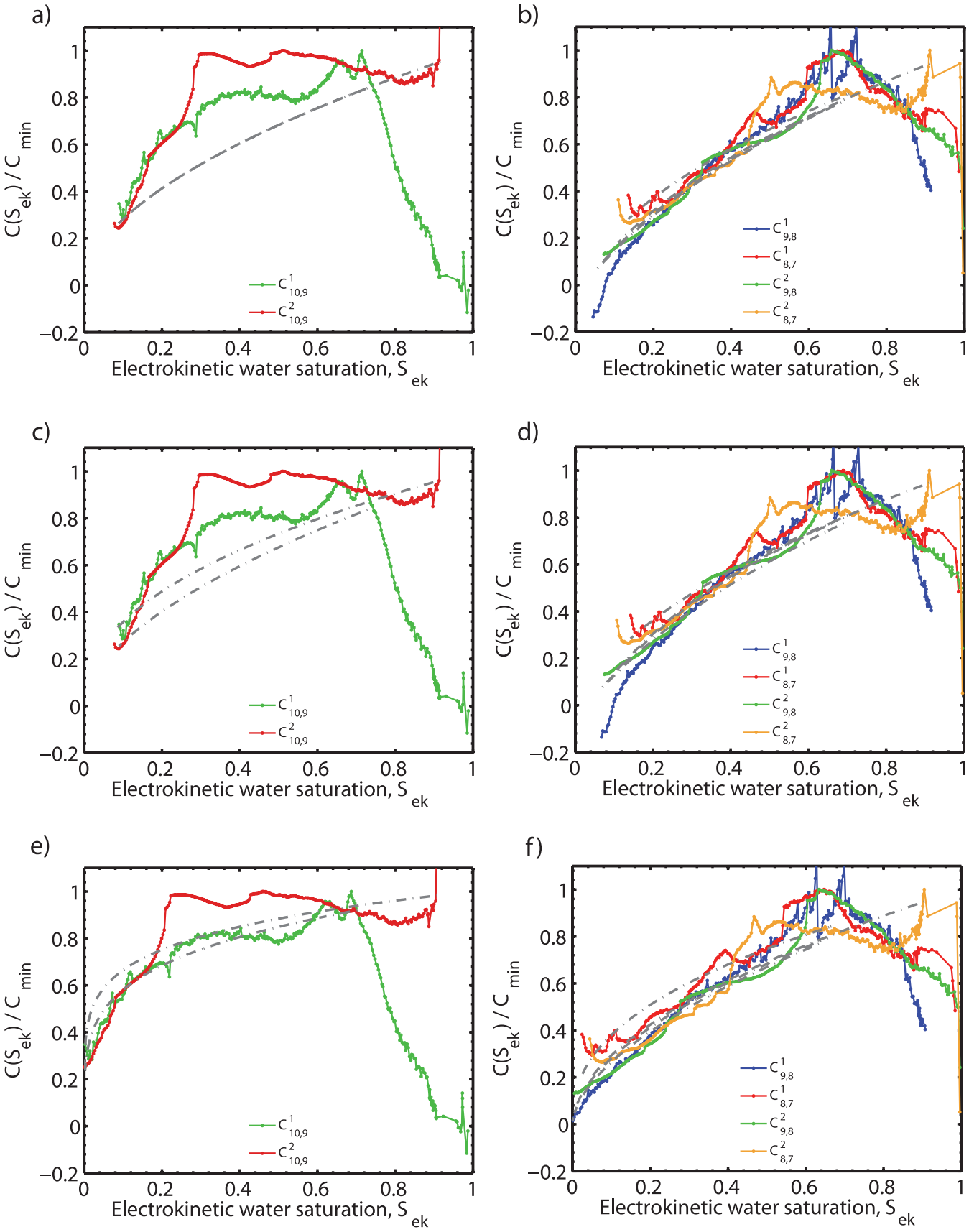

Figure 10. Fit of eqs (21), (22) and (25) for dipoles $C^1_{9,8}$, $C^1_{8,7}$, $C^2_{9,8}$ and $C^2_{8,7}$ (b, d, f), and for dipoles $C^1_{10,9}$, $C^2_{10,9}$ (a, c, e). See Table 5 for the values of β and $S_w^{r,ek}$.

Table 5. Fitted parameters of eqs (21), (22) and (25) compared to our data set.

	eq. (21)	eq. (22)	eq. (25)	
	$S_w^{r,ek}$	$S_w^{r,ek}$	$S_w^{r,ek}$	β_{ek}
$C^1_{10,9}$	/	/	0.088	0.24
$C^1_{9,8}$	0.064	0.04	0.13	0.55
$C^1_{8,7}$	0.019	0.011	0.13	0.42
$C^2_{10,9}$	/	/	0.09	0.18
$C^2_{9,8}$	0.059	0.57	0.12	0.57
$C^2_{8,7}$	0.05	0.053	0.11	0.53
	Number of monolayers			
$C^1_{10,9}$	/	/	2.4	
$C^1_{9,8}$	1.73	1.08	3.74	
$C^1_{8,7}$	0.51	0.3	3.59	
$C^2_{10,9}$	/	/	2.5	
$C^2_{9,8}$	1.62	1.57	3.39	
$C^2_{8,7}$	1.37	1.46	3.17	

Note: The value $n = 1.45$ is used for the Archie saturation exponent.

thickness and that covers all the surface area of pores. Although the interface is composed of an EDL rather than monolayers in saturated conditions (Revil & Glover 1997), this approach gives the possibility to roughly estimate the thickness of the adsorbed layer expected at different electrokinetic residual saturation $S_w^{r,ek}$. We estimated the internal surface area of the sand, from its technical specifications, to be 11.3 $m^2\,kg^{-1}$. Taking 0.35 nm as the thickness of a monolayer of water (Thorp 1959), we computed the equivalent number of monolayers of water (Table 5) corresponding to the fitted values of $S_w^{r,ek}$. These values constitute the thickness of the adsorbed water at the grain surface. The equivalent numbers of monolayers inferred from adjusted $S_w^{r,ek}$ of the Table 5 for eq. (25), vary from 2.4 to 3.74, which corresponds to thickness from 0.84 nm to 1.31 nm. One monolayer of water would correspond to electrokinetic residual saturation of 0.04, which could be considered as a minimum value of $S_w{}^{r,ek}$. On the other hand, Knight (1991) considered that a thickness of 0.5 monolayer of water is possible. This would lead to a minimum value of $S_w{}^{r,ek}$ of 0.02. Physically, the introduction of $S_w^{r,ek}$ involves the possibility of electrokinetics to appear while water flow is too small to be measured. Therefore the electrokinetics occurring at such low saturations appear within the residual water.

Then, considering the electrical double layer model in the 'thin double layer approximation' (or Debye approximation), we computed the so-called Debye length, which is a measure of the diffuse double layer thickness,

$$\chi = \sqrt{\frac{\epsilon k_B T}{e^2 C}}, \tag{26}$$

where k_B is the Bolztmann's constant, T is the temperature in Kelvin, e is the elementary charge (C) and C is the concentration equivalent to the ions per unit of volume deduced from electrical conductivity measurements. For measured $\sigma_w = 103.2 \times 10^{-4}$ S m^{-1} (first experiment) and $\sigma_w = 66.4 \times 10^{-4}$ S m^{-1} (second experiment), we computed $\chi \simeq 15$ nm. These values are in good agreement with the values published in the literature for such electrolyte concentrations (Pride 1994).

We point out that the values of the electrokinetic residual saturation deduced from our experiments are ranging between 0.09 and 0.13 (using eq. 25). The thickness of adsorbed water layer corresponding to $S_w{}^{r,ek}$ is about 1 nm, which is below the electrical double layer thickness in saturated state of $\simeq$15 nm.

6 CONCLUSIONS

An unexpected behaviour of the electrokinetic coefficient has been presented in this work. Indeed, it has been shown that the normalized electrokinetic coefficient increases and then decreases when water saturation decreases during a drainage, with a maximum of $C(S_w)/C_{min}$ for $S_w = 0.65 - 0.8$. We have demonstrated by using inverse hydraulic parameters, that existing models could not explain this complex behaviour. We propose first that an empirical power law, as $\alpha S_e{}^{\beta}$, could model electrokinetic coefficient data. Moreover, we introduce the concept of the electrokinetic residual saturation $S_w^{r,ek}$. Using this parameter, and although only this parameter is adjusted, it allows us to better fit our data set and to propose a new model (eq. 25). We show that the values of $S_w{}^{r,ek}$ are roughly 0.1, which would correspond to a thickness of adsorbed water of about 1 nm. Most of the values of the β_{ek} exponent are in the range 0.4–0.6 for saturation up to 0.8. Other drainage experiments are needed to confirm the model that we propose. Streaming potential and hydrodynamic measurements should be jointly inverted, taking into account electrical conductivity variations, in order to deduce a robust law of the electrokinetic coefficient behaviour in unsaturated conditions. Further studies should explain the underlying physical processes in the whole range of saturation. The comparison between drainage and imbibition experiments should give some pieces of explanations.

ACKNOWLEDGMENTS

This work was supported by the French National Scientific Center (CNRS), by ANR-TRANSEK, and by REALISE the 'Alsace Region Research Network in Environmental Sciences in Engineering' and the Alsace Region. We thank P. W. Glover and an anonymous reviewer for their very constructive reviews. The authors would like to thank M. Pierre-Daniel Matthey for his useful advises during the experiment conception, and M. Julien Allègre for his contribution in the numerical design of the experimental setup.

REFERENCES

Adler, P.M., Thovert, J.-F., Jacquin, C., Morat, P. & Moul, J.-L.L., 1997. Electrical signals induced by the atmospheric pressure variations in unsaturated media, *C.R. Acad. Sci. Paris, serie IIa,* **324,** 711–718.

Ahmad, M.U., 1964. A laboratory study of streaming potentials, *Geophys. Prospect.,* **12,** 49–64.

Archie, G.E., 1942. The electrical resistivity log as an aid in determining some reservoir characteristics, *Trans. Am. Inst. Min. Metall. Pet. Eng.,* pp. 146–154.

Bogolovsky, V.A. & Ogilvy, A.A., 1970. Natural potential anomalies as a quantitive index of the rate of seepage from water reservoirs, *Geophys. Prospect.,* **18,** 261–268.

Bordes, C., Jouniaux, L., Dietrich, M., Pozzi, J.-P. & Garambois, S., 2006. First laboratory measurements of seismo-magnetic conversions in fluid-filled fontainebleau sand, *Geophys. Res. Lett.,* **33,** L01302, doi:10.1029/2005GL024582.

Bordes, C., Jouniaux, L., Garambois, S., Dietrich, M., Pozzi, J.-P. & Gaffet, S., 2008. Evidence of the theoretically predicted seismo-magnetic conversion, *Geophys. J. Int.,* **174,** 489–504.

Brooks, R.J. & Corey, A.T., 1964. Hydraulic properties of porous media, *Hydrol. Pap.,* **3,** 318–333.

Carsel, R.F. & Parrish, R.S., 1988. Developing joint probability distributions of soil water retention characteristics, *Water Resour. Res.,* **24**(5), 755–769.

Corey, A.T., 2002. Simultaneous determination of water transmission and retention properties. Direct methods, in *Methods of Soil Analysis. Part 4. Physical Methods,* Vol. 5, eds Dane, J.H. & Topp, G.C., Soil Science Society of America, Inc., Madison, WI.

Darnet, M. & Marquis, G., 2004. Modelling streaming potential (sp) signals induced by water movement in the vadose zone, *J. Hydrol.,* **285,** 114–124.

Darnet, M., Marquis, G. & Sailhac, P., 2003. Estimating aquifer hydraulic properties from the inversion of surface streaming potential (sp) anomalies, *Geophys. Res. Lett.,* **30,** 1679.

Darnet, M., G. Marquis, & Sailhac, P., 2006. Hydraulic stimulation of geothermal reservoirs:fluid flow, electric potential and microseismicity relationships, *Geophys. J. Int.,* **166,** 438–444.

Davis, J.A., James, R.O. & Leckie, J., 1978. Surface ionization and complexation at the oxide/water interface, *J. Colloid Interface Sci.,* **63,** 480–499.

Doussan, C., Jouniaux, L. & Thony, J.-L., 2002. Variations of self-potential and unsaturated flow with time in sandy loam and clay loam soils, *J. Hydrol.,* **267,** 173–185.

Dukhin, S.S. & Derjaguin, B.V., 1974. Electrokinetic phenomena, in *Surface and Colloid Science,* Vol. 7, p. 322, ed. Matijevic, E., John Wiley and Sons, New York.

Finizola, A., Sortino, F., Lenat, J.-F. & Valenza, M., 2002. Fluid circulation at stromboli volcano (aeolian islands, italy) from self potential and co2 surveys, *J. Volc. Geotherm. Res.,* **116,** 1–18.

Finizola, A., Lenat, J.-F., Macedo, O., Ramos, D., Thouret, J.-C. & Sortino, F., 2004. Fluid circulation and structural discontinuities inside Misti volcano (Peru) inferred from sel-potential measurements, *J. Volc. Geotherm. Res.,* **135**(4), 343–360.

Garambois, S. & Dietrich, M., 2001. Seismoelectric wave conversions in porous media: field measurements and transfer function analysis., *Geophysics,* **66,** 1417–1430.

Garambois, S. & Dietrich, M., 2002. Full waveform numerical simulations of seismoelectromagnetic wave conversions in fluid-saturated stratified porous media., *J. geophys. Res.,* **107**(B7), ESE 5–1–ESE 5–18.

Gaskin, G.J. & Miller, J.D., 1996. Measurement of soil water content using a simplified impedance measuring technique, *J. Agric. Eng. Res.,* **63,** 153–160.

Gibert, D. & Pessel, M., 2001. Identification of sources of potential fields with the continuous wavelet transform: application to self-potential profiles, *Geophys. Res. Lett.,* **28,** 1863–1866.

Glover, P.W.J. & Walker, E., 2009. Grain-size to effective pore-size transformation derived from electrokinetic theory, *Geophysics,* **74,** E17–E29.

Glover, P.W.J., Zadjali, I.I. & Frew, K.A., 2006. Permeability prediction from MICP and NMR data using an electrokinetic approach, *Geophysics,* **71,** F49–F60.

Guichet, X., Jouniaux, L. & Pozzi, J.-P., 2003. Streaming potential of a sand column in partial saturation conditions, *J. geophys. Res.,* **108**(B3), 2141, doi:10.1029/2001JB001517.

Guichet, X., Jouniaux, L. & Catel, N., 2006. Modification of streaming potential by precipitation of calcite in a sand-water system: laboratory measurements in the ph range from 4 to 12, *Geophys. J. Int.,* **166,** 445–460.

Hase, H., Ishido, T., Takakura, S., Hashimoto, T., Sato, K. & Tanaka, Y., 2003. Zeta potential measurement of volcanic rocks from aso caldera, *Geophys. Res. Lett.,* **23**(30), 2210, doi:10.1029/2003GL018694.

Haverkamp, R., Leij, F.J., Fuentes, C., Sciortino, A. & Ross, P.J., 2005. Soil water retention: I. Introduction of a shape index, *Soil Sci. Soc. Am. J.,* **69,** 1881–1890.

Hayek, M., Lehmann, F. & Ackerer, P., 2007. Adaptative multi-scale parametrization for one-dimensional flow in unsaturated porous media, *Adv. Water Resour.,* **31**(1), 28–43, doi:10.1016/j.advwatres.2007.06.009

Henry, P., Jouniaux, L., Screaton, E.J., Hunze, S. & Saffer, D.M., 2003. Anisotropy of electrical conductivity record of initial strain at the toe of the nankai accretionary wedge, *J. geophys. Res.,* **108**(B9), ETG 2–1–ETG 2–12.

Hopmans, J., Simunek, J., Romano, N. & Durner, W., 2002. Simultaneous determination of water transmission and retention properties. Direct methods, in *Methods of Soil Analysis. Part 4. Physical Methods,* Vol. 5, eds Dane, J.H. and Topp, G.C., Soil Science Society of America, Inc., Madison, WI.

Ishido, T., 2004. Electrokinetic mechanism for the w-shaped self-potential profile on volcanoies, *Geophys. Res. Lett.,* **31,** L15616, doi:10.1029/2004GL020409.

Ishido, T. & Mizutani, H., 1981. Experimental and theoretical basis of electrokinetic phenomena in rock water systems and its applications to geophysics, *J. geophys. Res.,* **86,** 1763–1775.

Jaafar, M.Z., Vinogradov, J. & Jackson, M.D., 2009. Measurement of streaming potential coupling coefficient in sandstones saturated with high salinity NaCl brine, *Geophys. Res. Lett.,* **36,** L21306, doi:10.1029/2009GL040549.

Jackson, M.D., 2008. Characterization of multiphase electrokinetic coupling using a bundle of capillary tubes model, *J. geophys. Res.,* **113,** B04201, doi:10.1029/2007JB005490.

Jackson, M.D., 2010. Multiphase electrokinetic coupling: Insights into the impact of fluid and charge distribution at the pore scale from a bundle of capillary tubes model, *J. geophys. Res.,* **115,** B07206, doi:10.1029/2009JB007092.

Jouniaux, L. & Pozzi, J.-P., 1997. Laboratory measurements anomalous 0.1-0.5 hz streaming potential under geochemical changes: implications for electrotelluric precursors to earthquakes, *J. geophys. Res.,* **102,** 15 335–15 343.

Jouniaux, L., Lallemant, S. & Pozzi, J., 1994. Changes in the permeability, streaming potential and resistivity of a claystone from the Nankai prism under stress, *Geophys. Res. Lett.,* **21,** 149–152.

Jouniaux, L., Pozzi, J.-P., Berthier, J. & Massé, P., 1999. Detection of fluid flow variations at the Nankai trough by electric and magnetic measurements in boreholes or at the seafloor, *J. geophys. Res.,* **104,** 29 293–29 309.

Jouniaux, L., Bernard, M.-L., Zamora, M. & Pozzi, J.-P., 2000. Streaming potential in volcanic rocks from mount peleé, *J. geophys. Res.,* **105,** 8391–8401.

Knight, R., 1991. Hysteresis in the electrical resistivity of partially saturated sandstones, *Geophysics,* **56**(12), 2139–2147.

Lehmann, F. & Ackerer, P., 1998. Comparison of iterative methods for improved solutions of the fluid flow equation impartially saturated porous media, *Trans. Porous Media,* **31,** 275–292.

Leij, F.J., Haverkamp, R., Fuentes, C., Zatarain, F. & Ross, P.J., 2005. Soil water retention: II. Derivation and application of shape index, *Soil Sci. Soc. Am. J.,* **69,** 1891–1901.

Lesmes, D.P. & Friedman, S.P., 2006. Relationships between the electrical and hydrogeological properties of rocks and soils, in *Hydrogeophysics,* eds Rubin, Y. and Hubbard, S., Springer, Dordrecht.

Li, S.X., Pengra, D.B. & Wong, P., 1995. Onsager's reciprocal relation and the hydraulic permeability of porous media, *J. geophys. Res.,* **51**(6), 5748–5751.

Linde, N., Jougnot, D., Revil, A., Matthai, S.K., Renard, D. & Doussan, C., 2007. Streaming current generation in two-phase flow conditions, *Geophys. Res. Lett.,* **34,** LO3306, doi:10.1029/2006GL028878.

Lorne, B., Perrier, F. & Avouac, J.-P., 1999a. Streaming potential measurements. 1. Properties of the electrical double layer from crushed rock samples, *J. geophys. Res.,* **104**(B8), 17 857–17 877.

Maineult, A., Bernabé, Y. & Ackerer, P., 2004. Electrical response of flow, diffusion and advection in a laboratory sand box, *Vadose Zone J.,* **3,** 1180–1192.

Maineult, A., Bernabé, Y. & Ackerer, P., 2005. Detection of advected concentration and ph fronts from self-potential measurements, *J. geophys. Res.,* **110,** B11205, doi:10.1029/2005JB003824.

Maineult, A., Strobach, E. & Renner, J., 2008. Self-potential signals induced by periodic pumping test, *J. geophys. Res.,* **113,** B01203, doi:10.1029/2007JB005193.

Marquis, G., Darnet, M., Sailhac, P., Singh, A.K. & Gérard, A., 2002. Surface electric variations induced by deep hydraulic stimulation: an example from the Soultz HDR site, *Geophys. Res. Lett.,* **29,** doi:10.1029/2002GL015046.

Marshall, D.J. & Madden, T.R., 1959. Induced polarization, a study of its causes, *Geophysics,* **24**(4), 790–816.

Massenet, F. & Pham, V.N., 1985. Experimental and theoretical basis of self-potential phenomena in volcanic areas with reference to results obtained on Mount Etna, *Earth planet. Sci. Lett.,* **73,** 415–429.

Morgan, F.D., Williams, E.R. & Madden, T.R., 1989. Streaming potential properties of westerly granite with applications, *J. geophys. Res.,* **94**(B9), 12 449–12 461.

Mualem, Y., 1976a. A new model for predicting the hydraulic conductivity of unsaturated porous media, *Water Resour. Res.,* **12,** 513–522.

Naudet, V., Revil, A., Bottero, J.-Y. & Bégassat, P., 2003. Relationship between self-potential (SP) signals and redox conditions in contaminated groundwater, *Geophys. Res. Lett.,* **30**(21), HLS 2-1–HLS 2-4.

Onizawa, S., Matsushima, N., Ishido, T., Hase, H., Takakura, S. & Nishi, Y., 2009. Self-potential distribution on active volcano controlled by three-dimensional resistivity structure in izu-oshima, japan, *Geophys. J. Int.,* **178,** 1164–1181.

Onsager, L., 1931. Reciprocical relation in irreversible processes: I, *Phys. Rev,* **37**(4), doi:10.1103/PhysRev.37.405.

Overbeek, J.T.G., 1952. Electrochemistry of the double layer., in *Colloid Science, Irreversible Systems,* Vol. 1, pp. 115–193, ed. Kruyt, H.R., Elsevier, New York.

Pengra, D.B., Li, S.X. & Wong, P., 1999. Determination of rock properties by low frequency ac electrokinetics, *J. geophys. Res.,* **104**(B12), 29 485–29 508.

Perrier, F. & Froidefond, T., 2003. Electrical conductivity ans streaming potential coefficient in a moderately alkaline lava series, *Earth planet. Sci. Lett.,* **210,** 351–363.

Perrier, F. & Morat, P., 2000. Characterization of electrical daily variations induced by capillary flow in the non-saturated zone, *Pure appl. Geophys,* **157,** 785–810.

Pezard, P., Gautier, S., Borgne, T.L., Legros, B. & Deltombe, J.-L., 2009. Muset: a multiparameter and high precision sensor for downhole spontaneous electrical potential measurements, *Comptes Rendus - Geosci.,* **341,** 957–964.

Pinder, G.F. & Gray, W.G., 1977. *Finite Element Simulation in Surface and Subsurface Hydrology,* Academic Press, New York.

Pozzi, J.-P. & Jouniaux, L., 1994. Electrical effects of fluid circulation in sediments and seismic prediction, *C.R. Acad. Sci. Paris, Ser. II,* **318**(1), 73–77.

Pride, S., 1994. Governing equations for the coupled electromagnetics and acoustics of porous media, *Phys. Rev. B,* **50,** 15 678–15 695.

Pride, S. & Morgan, F.D., 1991. Electrokinetic dissipation induced by seismic waves, *Geophysics,* **56**(7), 914–925.

Rawls, W.J., Brakensiek, D.L. & Saxton, K.E., 1982. Estimation of soil water properties, *Trans. ASAE,* **25,** 1316–1320.

Revil, A. & Glover, P.W., 1997. Theory of ionic-surface electrical conduction in porous media, *Phys. Rev. B,* **55**(3), 1757–1773.

Revil, A., Pezard, P.A. & Glover, P.W.J., 1999a. Streaming potential in porous media: 1. Theory of the zeta potential, *J. geophys. Res.,* **104**(B9), 20 021–20 031.

Revil, A., Linde, N., Cerepi, A., Jougnot, D., Matthai, S. & Finsterle, S., 2007. Electrokinetic coupling in unsaturated porous media, *J. Colloid Interface Sci.,* **313,** 315–327.

Richards, L.A., 1931. Capillary conduction of liquids through porous medium, *Physics,* **1,** 318–333.

Rivière, A., 1977. *Méthodes granulométriques: Techniques et interpr(c)tations,* Masson, Paris.

Sailhac, P. & Marquis, G., 2001. Analytic potentials for the forward and inverse modeling of SP anomalies caused by subsurface fluid flow, *Geophys. Res. Lett.,* **28,** 1851–1854.

Sailhac, P., Darnet, M. & Marquis, G., 2004. Electrical streaming potential measured at the ground surface: forward modeling and inversion issues for monitoring infiltration and characterizing the vadose zone, *Vadose Zone J.,* **3,** 1200–1206.

Saunders, J.H., Jackson, M.D. & Pain, C.C., 2008. Fluid flow monitoring in oilfields using downhole measurements of electrokinetic potential, *Geophysics,* **73,** E165–E180.

Schön, J., 1996. *Physical Properties of Rocks—Fundamentals and Principles of Petrophysics,* Vol. 18, Elsevier Science Ltd., Handbook of Geophysical Exploration, Seismic Exploration.

Smoluchowski, M., 1905. Zur theorie der elektrischen kataphorese und der oberflchenleitung, *Physikalische Z,* **6,** 529–536.

Sprunt, E.S., M., T.B. & Djabbarah, N.F., 1994. Streaming potential from multiphase flow, *Geophysics,* **59**(5), 707–711.

Stern, O., 1924. Zur theorie der electrolytischen doppelschicht, *Z. Electrochem.,*(30), 508–516.

Strahser, M.H., Rabbel, W. & Schildknecht, F., 2007. Polarisation and slowness of seismoelectric signals: a case study, *Near Surf. Geophys.,* **5,** 97–114.

Thorp, J.M., 1959. The dielectric behaviour of vapors adsorbed on porous solids, *Trans. Faraday. Soc.,* **55,** 442.

Titov, K., Revil, A., Konosavsky, P., Straface, S. & Troisi, S., 2005. Numerical modelling of self-potential signals associated with a pumping test experiment, *Geophys. J. Int.,* **162,** 641–650.

Tosha, T., Matsushima, N. & Ishido, T., 2003. Zeta potential measured for an intact granite sample at temperatures to 200c, *Geophys. Res. Lett.,* **30**(6), 1295, doi:10.1029/2002GL016608.

APPENDIX A: INSTRUMENTAL AND EXTERNAL FACTORS INFLUENCING SP MEASUREMENTS

We present in this section some test experiments carried out to investigate the different sources of electrical noise on SP measurements. This noise could be induced by acquisition process or by experimental setup.

The first experiments were performed in water to study the influence of water content probes on SP measurements. Actually these probes apply an electrical field to perform the measurements and it could perturb the streaming potential measurements. Some SP measurements were combined to water content measurements (black and red curve) and compared to SP alone (green curve) (Fig. A1). The shielded part of SP electrode's cables is connected to a secure ground point on the acquisition unit. We observe that the high

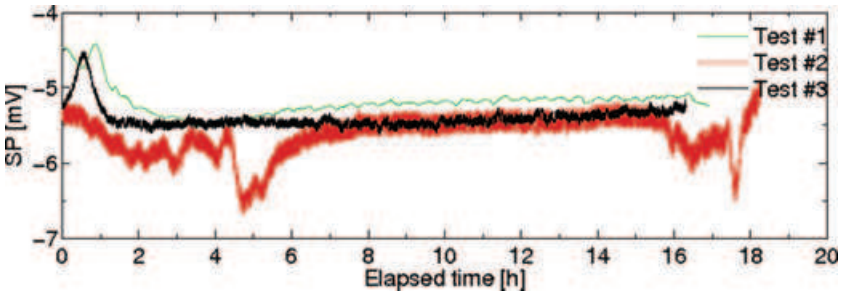

Figure A1. SP signals measured in water without any other measurements (green curve) and SP measurements combined to water content measurements, without the ground connection (red curve), and integrated on 100 periods of 50 Hz (black curve).

frequency noise increases when water content is measured. The amplitude of this noise is around 0.2 mV, which is negligible in regards to the typical SP values presented in this paper. In order to reject anthropogenic noise, the signals are integrated on several periods of the 50 Hz signal. The black signal on the Figure is integrated on 100 periods of the 50 Hz, corresponding to 2 s of measurement, and the red one is integrated on 10 periods only. The impact of this integration is important, so that we chose to integrate all SP measurements on 100 periods of the 50 Hz for each experiment. Finally, some more larger fluctuations (around 1 mV) are identified on the red curve, with a 12 hr delay. These variations are linked to temperature fluctuations which are detailed below.

Finally, water content probes have been placed into the column 5 cm (see Fig. 1) from SP electrodes to minimize their effects.

The same experimental protocol was used to fill the column to ensure the repeatability of all experiments. The column has been filled by imbibition in order to limit the formation of air bubbles and to ensure a uniform paking. When the sand is dropped into the column, the water volume is maintained larger than the sand volume. Thus, the medium remains saturated and the water content is uniform in the whole column. Finally, a first test drainage is carried out to ensure the sand packing.

The chemical equilibrium stability of the mixture (sand with water) and temperature fluctuations have been monitored during the equilibrium phase, before the drainage experiment. The water electrical conductivity, σ_w, and pH during the chemical equilibrium phase (described in the Section 3) are measured in the stocked water and in the outflow water, which is the water sampled at the column exit after flow (Fig. A2). We observe the stabilization of both σ_w and pH values after recycling the pore volume four times. This stabilization, considering the measurement accuracy, is obtained after almost 7 d, in the same flow conditions than for the drainage experiment.

Temperature fluctuations have also been monitored, using two thermocouples, inside and outside the column during the first experiment (Fig. A3b), and are compared to raw SP measurements

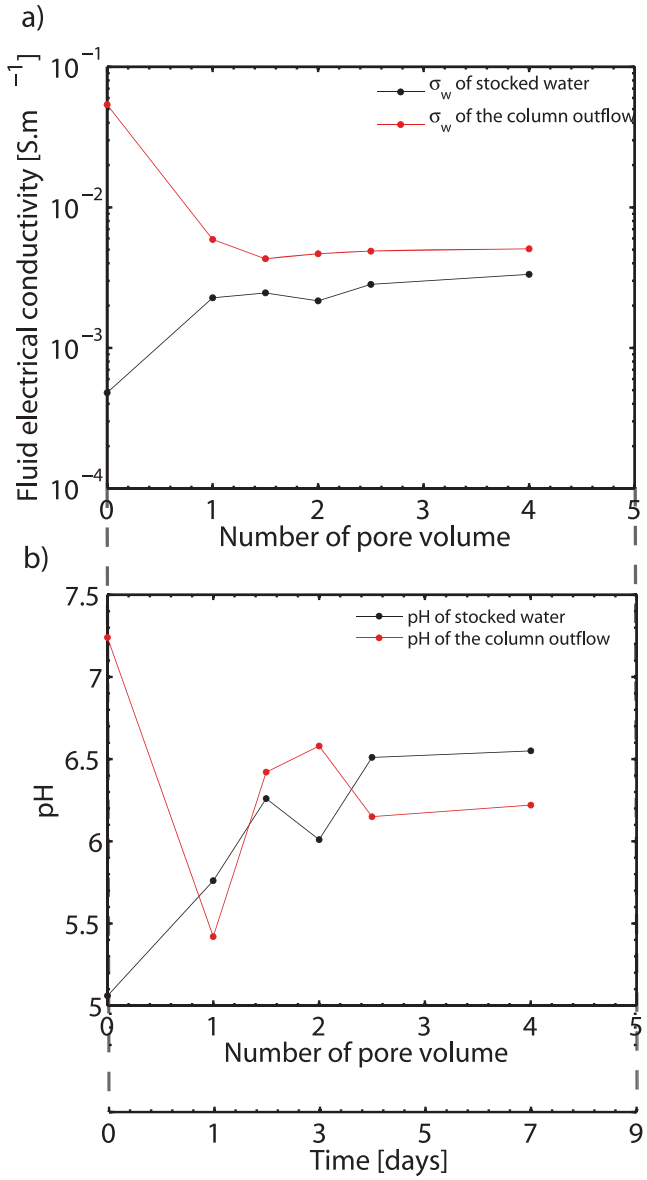

Figure A2. Water electrical conductivity and pH measured during the equilibrium phase of the first experiment, in the stocked water and in the outflow water. The flow conditions are the same than those during a drainage experiment.

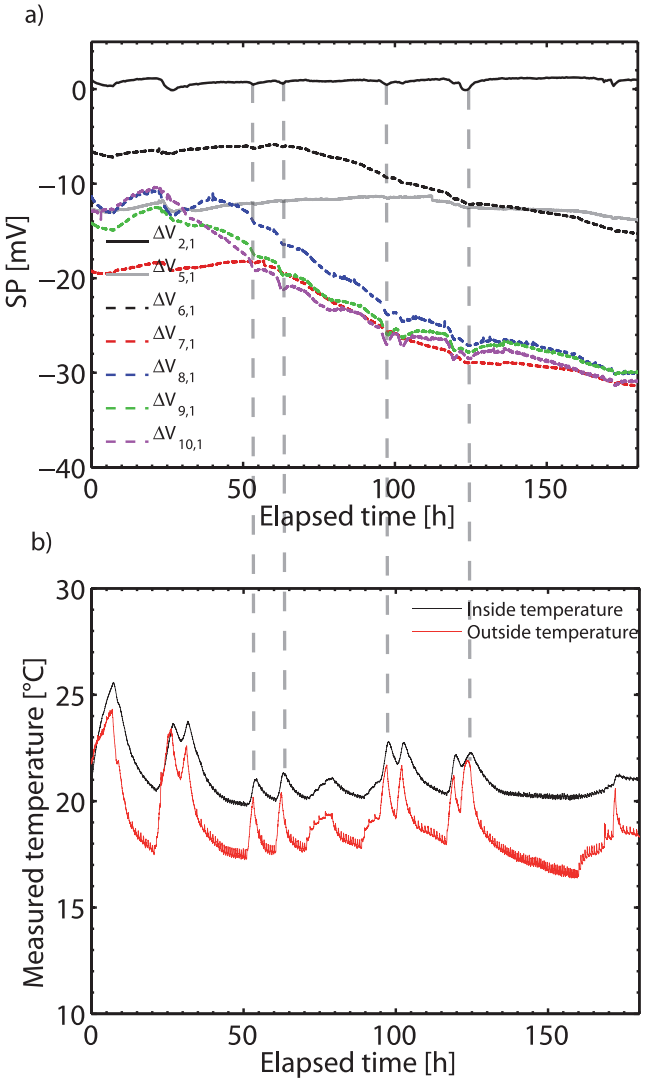

Figure A3. Raw SP measurements of the first experiment (a) and temperature monitored inside and outside the column at the same time (b).

(Fig. A3a). Some periodical variations linked to day/night cycles are clearly identified on the temperature measurements. The maximum value of temperature fluctuations inside the column is about 2 °C.

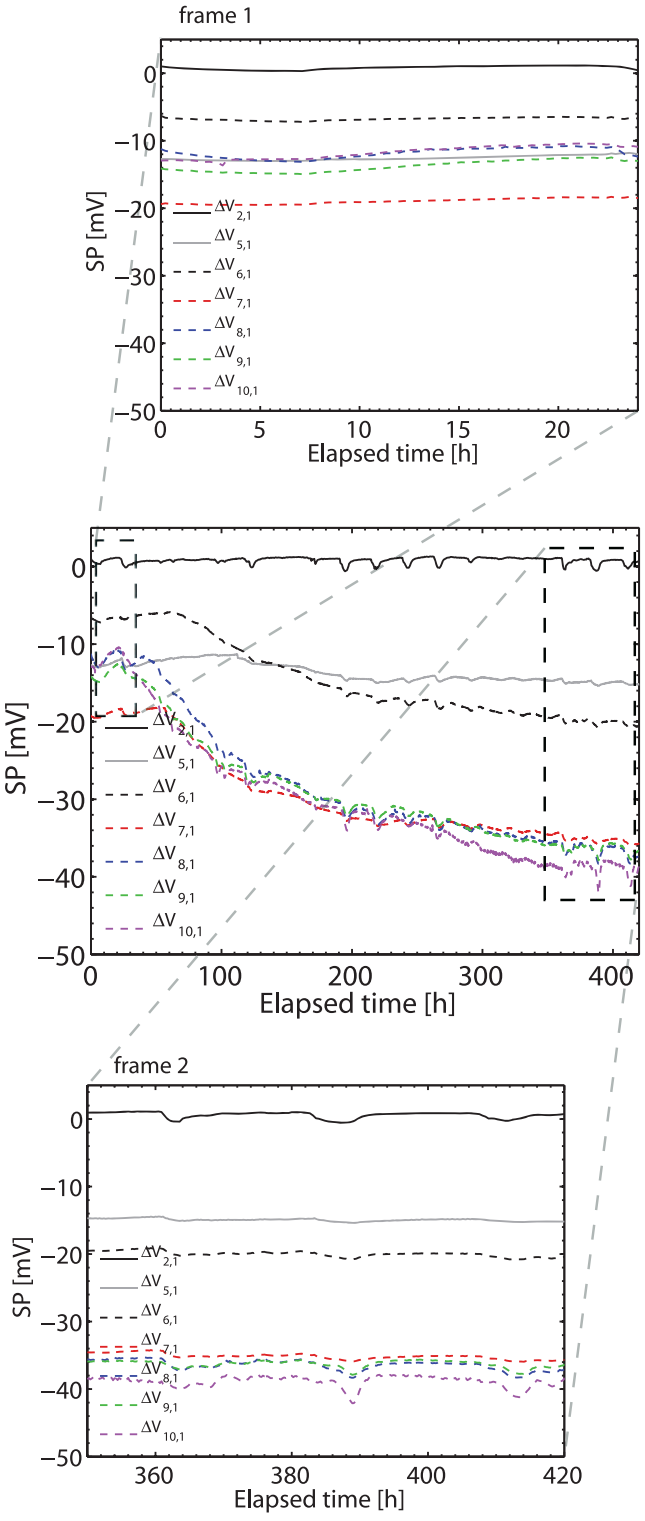

Figure A4. Raw SP measurements for the first experiment. The frame #1 is a zoom on the first 24 hr of the recording (before the drainage start), and the second frame is a zoom on the last 40 hr of the recording (after the flow stop).

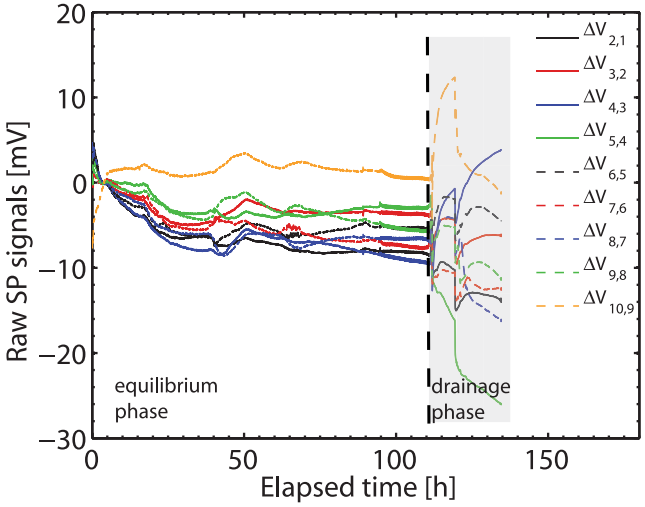

Figure A5. An example of experimental recording during the equilibrium phase. A 30 hr stable phase is identified just before the drainage start.

Corresponding peaks in the raw SP signals are identified by dashed lines (Fig. A3) and clearly correlated to temperature. However, the noise amplitude involved in SP data by temperature fluctuations is negligible, in regards to characteristic SP signals measured during a drainage experiment.

The two experiments presented in this paper are very long (around 300–400 hr), so that it is important not to have a drift in the SP signals.

Raw SP recordings of the first experiment are reported (Fig. A4). The first frame represents almost 24 hr of measurements before the drainage start. The second frame represents more than 40 hr of measurements after the drainage stopped. These two examples show a very stable SP signals for all dipoles when there is no water flow. Moreover, the SP measured with the dipole (2, 1) is stable around 1 mV for 400 hr of recording, as we could expect in the part of the column which remains saturated. These examples reject the possibility of electrodes drifting during the experiment and attest their accuracy.

Another example of a long raw SP recording before a drainage experiment not presented in this paper shows a quite stable electrical potential values during 50 hr after a long equilibrium phase (Fig. A5). This example is representative of recorded signals of different phases during an experiment.

We concluded from all these test experiments that the instrumental and external sources of electrical noise are small enough to allow us to detect a streaming potential induced by a drainage experiment.

APPENDIX B: ELECTRICAL AND ELECTROKINETIC CHARACTERIZATION OF THE SAND

The C_{sat} value can be measured in steady-state saturated flow. Streaming Potential (SP) is measured for several applied pore pressures within a sample of sand (Fig. B1a). These measurements were performed using another experimental setup (Jouniaux *et al.* 2000), to be able to apply large enough pressure differences (up to 30 000 Pa) to induce a measurable electrokinetic coefficient, which was -3×10^{-7} V Pa^{-1} (with $\sigma_w = 0.055$ S m^{-1}). The slope of the regression leads to the value of C_{sat}. These measurements have been made at a higher water salinity than the one observed in both experiments presented in this paper. Assuming that

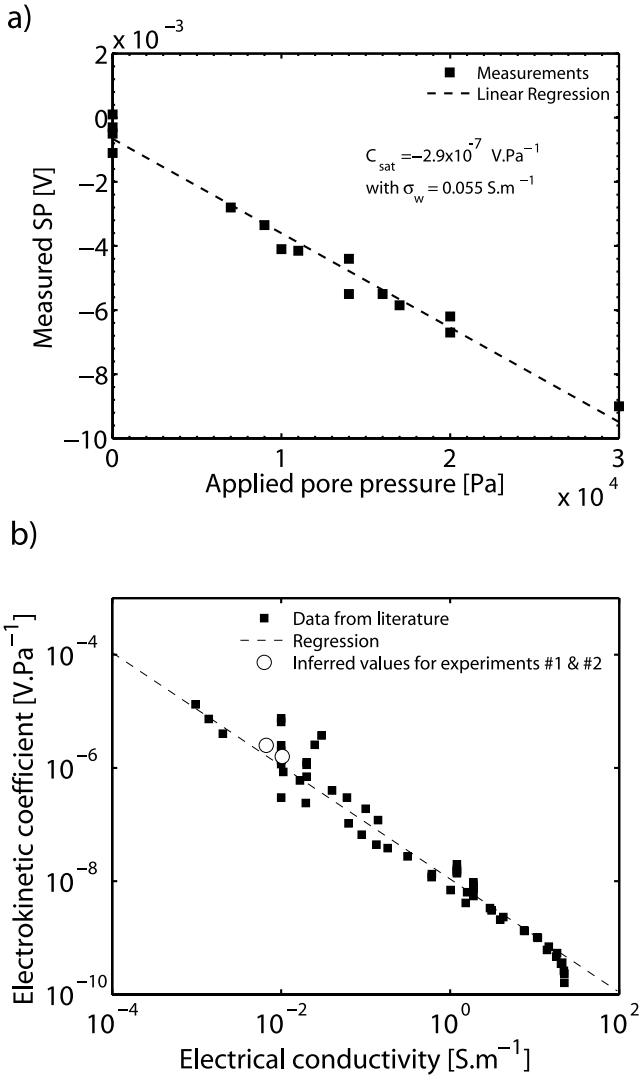

Figure B1. (a) SP measured on Sifraco NE34 sand sample. The slope of the regression (black dashed line) leads to the value of the electrokinetic coefficient at saturation, $C_{sat} = -2.9 \times 10^{-7}$ V Pa^{-1} for water conductivity $\sigma_w = 0.05 \times 10^{-2}$ S m^{-1}. (b) The inferred values of C_{sat} at conductivities used in experiment #1 and #2 (empty circles). Comparison with data collected (in absolute terms) on sands and sandstones at pH 7−8 (when available) from Ahmad (1964), Guichet *et al.* (2003, 2006), Ishido & Mizutani (1981), Jaafar *et al.* (2009), Jouniaux & Pozzi (1997), Li *et al.* (1995), Lorne *et al.* (1999a), Pengra *et al.* (1999), Perrier & Froidefond (2003). The regression (black dashed line) leads to $C_{sat} = -1, 1 \times 10^{-8} \cdot \sigma_w^{-1}$ V Pa^{-1}.

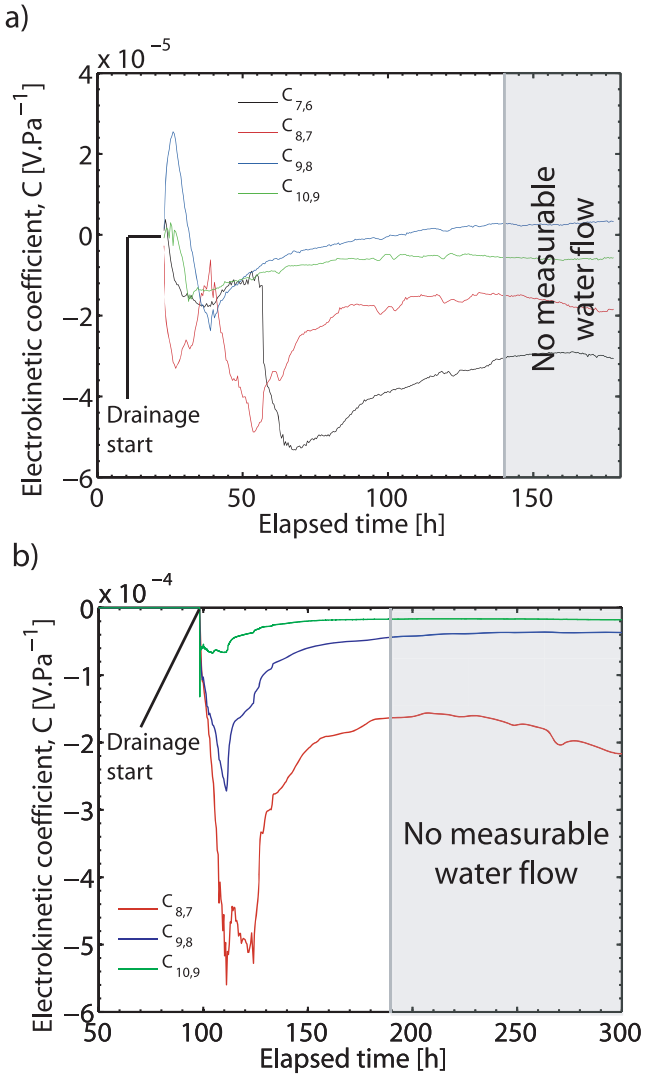

Figure B2. The raw electrokinetic coefficient measurements deduced from measured SP and computed ΔP, for experiment #1 (a), and for experiment #2 (b).

the Helmholtz–Smoluchowski equation is valid, we inferred the C_{sat} values corresponding to the conductivities of the two experiments of this paper. This calculation leads to $C_{sat} = -1.6 \times 10^{-6}$ V Pa^{-1} (with $\sigma_w = 103.2 \times 10^{-4}$ S m^{-1}) for the first one and $C_{sat} = -2.5 \times 10^{-6}$ V Pa^{-1} (with $\sigma_w = 66.4 \times 10^{-4}$ S m^{-1}) for the second one. Measurements of C_{sat} performed on sand and sandstone samples collected in the literature are shown as a function of the water electrical conductivity, σ_w (Fig. B1b). The regression leading to $C_{sat} = 10^{-8} \cdot \sigma_w^{-1}$ shows that our values of C_{sat} are in the general trend deduced from other studies on sand and sandstones.

Raw electrokinetic coefficient computed through eq. (2), using measured SP and computed ΔP (Figs 3 and 4 respectively), are reported (Figs B2a and b). No water flow was measurable at $\simeq$140 hr and $\simeq$190 hr after the drainage start for experiment #1 and #2 respectively. At this step, measured water-content and water pressures stopped to decrease and kept stable (see Fig. 2). Then, the minimum of water saturation was reached for all the dipoles. Thus, electrokinetic coefficient data presented as a function of water saturation in this paper correspond to $\simeq$140 hr and $\simeq$190 hr of measurements from the drainage start. We can also observe on these Figures the scattering of the measurements at the beginning of the experiment #1 which we detail below.

In addition, we propose a statistical study of our data set to estimate its uncertainty. We applied a sliding window to the $C(S_w)$ data set. The width of the window is defined in terms of water saturation interval $S_w = 0.05$. This value corresponds to the error on water saturation measurements. In each window we analysed the measurements distribution as an histogram. The obtained distributions were non-symmetric (as Gaussian distribution for instance), so that we decided to represent the median value of the distribution in each window (coloured circles in the Fig. B3). We computed the error bars using the minimum and the maximum value of $C(S_w)$ in each window. Thus, error bars include 100 per cent of the

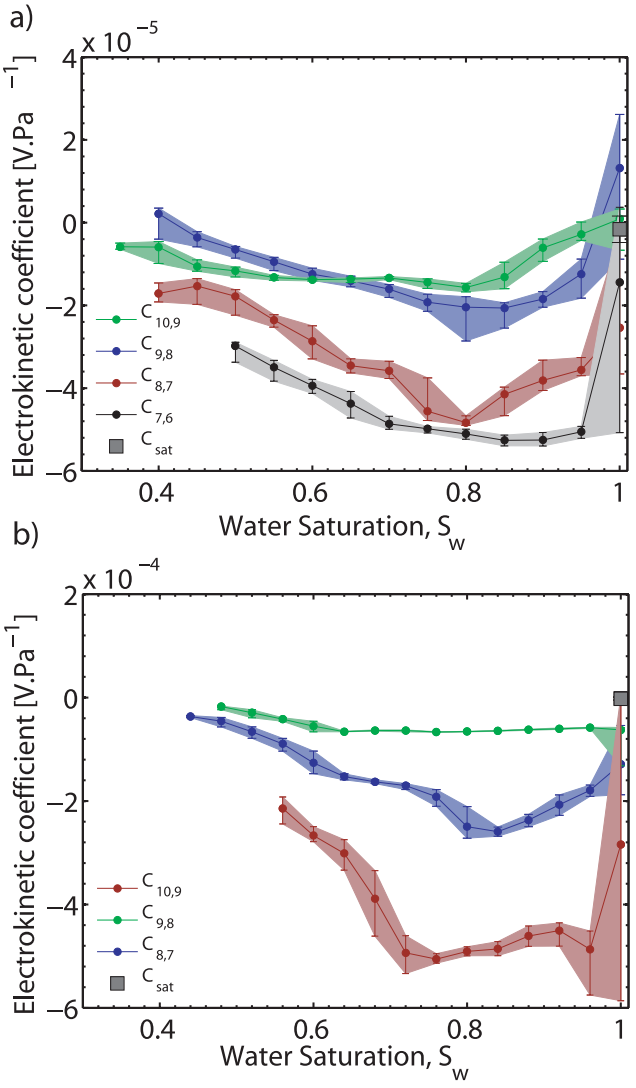

Figure B3. Statistical study of the raw electrokinetic coefficients for experiment #1 (a) and experiment #2 (b). A sliding window of $S_w = 0.05$ width is applied to the data set. The median of the distribution is chosen for each window to represent the data. The error bars correspond to the minimum and maximum values of the distribution for each window. The inferred values of C_{sat} are represented by squares.

uncertainty linked to all the noise sources we cannot control during the experiment.

The uncertainty is maximum at the beginning of each experiment (Fig. B3). We observe that the inferred C_{sat} is included in error bars.

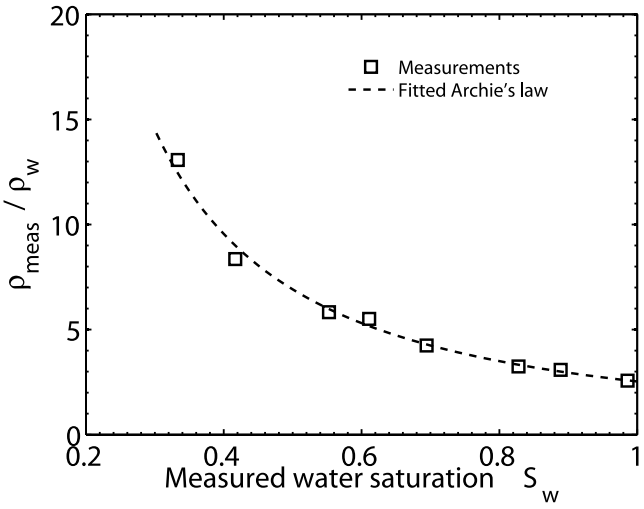

Figure B4. True electrical resistivity of the sand. The black squares are measured ρ_r/ρ_w for nine water/sand mixtures. The water-content was controlled by weight. The black dashed line is the best Archie's law fitting the data. Results lead to $n = 1.45$ for the Archie saturation exponent.

Furthermore, error bars also include the zero when some signals change in sign at very low saturations. This analysis confirms that our measurements are precise and accurate enough to follow the electrokinetic coefficient behaviour as a function of water saturation.

The electrokinetic coefficient models computed in Section 5 need the Archie saturation exponent n to be known. Rather than to choose n from some published values, we decided to measure electrical resistivity of the unsaturated sand in a small-scale column (already used for Theta probe calibrations). Nine sand mixtures were prepared by weight to obtain nine different homogeneous unsaturated media. The values of θ varies from θ_r to θ_s to ensure a good coverage of the whole saturation domain. We also measured the porosity (equivalent to θ_s) which was equal to 0.36. Measurements of electrical resistance were carried out with circular stainless steel (same diameter than the column) placed at each extremity, and using an impedancemeter (Agilent 4263b) combined with the same acquisition system than for experiments #1 and #2. Thus, the simple and short cylindrical geometry of this experiment allowed us to easily convert raw electrical resistance values in terms of true electrical resistivity ρ_{meas}. The values ρ_{meas} normalized by the measured water electrical resistivity are shown as a function of water saturation (Fig. B4). Then, Archie's law was fitted to the data in a least square sense, and results gave $n = 1.45$ for the second Archie exponent.